Interpreting canopy development and physiology using a European phenology camera network at flux sites

Running title: Linking ecosystem fluxes to canopy phenology in Europe

Lisa Wingate[1], Jérôme Ogée[1], Edoardo Cremonese[2], Gianluca Filippa[2], Toshie Mizunuma[3], Mirco Migliavacca[4], Christophe Moisy[1], Matthew Wilkinson[5], Christine Moureaux[6], Georg Wohlfahrt[7,29], Albin Hammerle[7], Lukas Hörtnagl[7,15], Cristina Gimeno[8], Albert Porcar-Castell[9], Marta Galvagno[2], Tatsuro Nakaji[10], James Morison[5], Olaf Kolle[4], Alexander Knohl[11], Werner Kutsch[12], Pasi Kolari[9], Eero Nikinmaa[9], Andreas Ibrom[13], Bert Gielen[14], Werner Eugster[15], Manuela Balzarolo[14,16], Dario Papale[16], Katja Klumpp[17], Barbara Köstner[18], Thomas Grünwald[18], Richard Joffre[19], Jean-Marc Ourcival[19], Margareta Hellstrom[20], Anders Lindroth[20], George Charles[21], Bernard Longdoz[22], Bernard Genty[23,24], Janne Levula[9], Bernard Heinesch[6], Michael Sprintsin[25], Dan Yakir[26], Tanguy Manise[6], Dominique Guyon[1], Hella Ahrends[15,27], Andrés Plaza-Aguilar[28], Jin Hong Guan[4], John Grace[3]

[1]INRA, UMR ISPA 1391 , 33140 Villenave d'Ornon, France

[2]Environmental Protection Agency of Aosta Valley, ARPA Valle d'Aosta, Climate Change Unit,

[3]School of GeoSciences, University of Edinburgh, Edinburgh, EH9 3JN, UK

[4]Max Planck Institute for Biogeochemistry, Jena, Germany

[5]Forest Research, Alice Holt, Farnham, GU10 4LH, UK

[6]Unite de Physique des Biosystemes, Gembloux Agro-Bio Tech, Université of Liège, 5030 Gembloux, Belgium

[7]University of Innsbruck, Innsbruck, Austria

[8]Centro de Estudios Ambientales del Mediterráneo, Paterna, Spain

[9]Department of Forest Sciences, University of Helsinki, P.O.Box 27, 00014 Finland

[10]University of Hokkaido, Hokkaido, Japan

[11]Georg-August University of Göttingen, 37077 Göttingen, Germany

[12]Johann Heinrich von Thünen-Institut (vTI) Institut für Agrarrelevante Klimaforschung, 38116 Braunschweig

[13]Risø National Laboratory for Sustainable Energy, Risø DTU, DK-4000 Roskilde, Denmark

[14]Department of Biology/Centre of Excellence PLECO, University of Antwerp, Antwerp, Belgium

[15]ETH Zurich, Institute of Agricultural Sciences, 8092 Zurich, Switzerland

[16]Department of Forest Environment and Resources, University of Tuscia, Viterbo, Italy.

[17]INRA, Grassland Ecosystem Research Unit, UR874, 63100 Clermont Ferrand, France

[18]Chair of Meterorology, Technische Universität Dresden, Tharandt, Germany

[19]CNRS, CEFE (UMR5175), Montpelier, France

[20]Department of Physical Geography and Ecosystem Science, Lund University, SE-22362 Lund, Sweden

[21]Centre for Ecology and Hydrology, Wallingford, Oxford, UK

[22]INRA, UMR EEF (UMR1137) Nancy, France

[23]CEA, IBEB, SVBME, Laboratoire d'Ecophysiologie Moléculaire des Plantes, 13108 Saint-Paul-lez-Durance, France

[24]CNRS, UMR Biologie Végétale et Microbiologie Environnementales (UMR7265), 13108 Saint-Paul-lez-Durance, France

[25]Israeli Forest Service,

[26]Weizmann Institute for Science, Rehovot, Israel

[27]Institute for Geophysics and Meteorology, University of Cologne, 50674 Cologne, Germany

[28]University of Cambridge, Cambridge, UK

[29]European Academy of Bolzano, 39100 Bolzano, Italy

Corresponding author:

Lisa Wingate

INRA-UMR 1391 ISPA

BP 81
33140 Villenave d'Ornon
France
phone: +33(0)55712 2431 / 2431, fax: +33(0)557122420
e-mail: lisa.wingate@bordeaux.inra.fr

Keywords: FLUXNET, phenology; PROSAIL; chlorophyll; photosynthesis; digital camera; green fraction; RGB analysis; NDVI

Abstract

Plant phenological development is orchestrated through subtle changes in photoperiod, temperature, soil moisture and nutrient availability. Presently, the exact timing of plant development stages and their response to climate and management practices are crudely represented in land surface models. As visual observations of phenology are laborious, there is a need to supplement long-term observations with automated techniques such as those provided by digital repeat photography at high temporal and spatial resolution. We present the first synthesis from a growing observational network of digital cameras installed on towers across Europe above deciduous and evergreen forests, grasslands and croplands, where vegetation and atmosphere CO_2 fluxes are measured continuously. Using colour indices from digital images and using piecewise regression analysis of time-series, we explored whether key changes in canopy phenology could be detected automatically across different land use types in the network. The piecewise regression approach could capture the start and end of the growing season, in addition to identifying striking changes in colour signals caused by flowering and management practices such as mowing.

Exploring the dates of green up and senescence of deciduous forests extracted by the piecewise regression approach against dates estimated from visual observations we found that these phenological events could be detected adequately (RMSE < 8 and 11 days for leaf out and leaf fall respectively). We also investigated whether the seasonal patterns of red, green and blue colour fractions derived from digital images could be modelled mechanistically using the PROSAIL model parameterised with information of seasonal changes in canopy leaf area and leaf chlorophyll and carotenoid concentrations. From a model sensitivity analysis we found that variations in colour fractions, and in particular the late spring 'green hump' observed repeatedly in deciduous broadleaf canopies across the network, are essentially dominated by changes in the respective pigment concentrations. Using the model we were able to explain why this spring maximum in green signal is often observed out of phase with the maximum period of canopy photosynthesis in ecosystems across Europe. Coupling such quasi-continuous digital records of canopy colours with co-located CO_2 flux measurements will improve our understanding of how changes in growing season length are likely to shape the capacity of European ecosystems to sequester CO_2 in the future.

1 Introduction

Within Europe continuous flux measurements of CO_2, water and energy exchange between ecosystems and the atmosphere started in the early 1990s at a handful of forest sites (Janssens et al., 2001; Valentini et al., 2000). Nowadays, through the realisation of large European programmes such as EUROFLUX and CARBOEUROPE-IP amongst others, the number of natural and managed terrestrial ecosystems where the dynamics of water and CO_2 fluxes are monitored continuously has increased tremendously (Baldocchi, 2014; Baldocchi et al., 2001), and that number is set to be maintained in Europe for at least the next twenty years as part of the European Integrated Carbon Observation System (ICOS, www.icos-infrastructure.eu/). This long-standing co-ordinated European network, placed across several important biomes, has already documented large inter-annual variability in the amount of CO_2 sequestered over the growing season (Delpierre et al., 2009b; Le Maire et al., 2010; Osborne et al., 2010; Wu et al., 2012) and witnessed both the short-lived and long-term impacts of disturbance (Kowalski et al., 2004), heat waves (Ciais et al., 2005) and management practices (Kutsch et al., 2010; Magnani et al., 2007; Soussana et al., 2007) on the carbon and water balance of terrestrial ecosystems. As a direct result of such an observational network, it is now possible to estimate with greater confidence how evapotranspiration (ET) and net ecosystem CO_2 exchange (NEE) have responded to changes in climate over recent years (Beer et al., 2010; Jung et al., 2010) and better constrain our predictions of how ecosystems are likely to respond in the future to changes in climate using land surface and biogeochemical cycle models (Friend et al., 2007; Krinner et al., 2005).

The growth of new leaves every year is clearly signalled in atmospheric CO_2 concentration records and exerts a strong control on both spatial and temporal patterns of carbon (C) sequestration and water cycling (Keeling et al., 1996; Piao et al., 2008). Hence, for the purpose of understanding patterns and processes controlling C and water budgets across a broad range of scales, there are obvious advantages in creating explicit links between flux monitoring, phenological observation and biogeochemical studies (Ahrends et al., 2009; Baldocchi et al., 2005; Kljun, 2006; Lawrence and Slingo, 2004; Richardson et al., 2007; Wingate et al., 2008). Leaf phenology has fascinated human observers for centuries and is related to external signals such as temperature or photoperiod (Aono and Kazui, 2008; Demarée and Rutishauser, 2009; Linkosalo et al., 2009). In the modern era, phenology has gained a new impetus, as people realised that such records must be sustained over many years to reveal subtle changes in plant phenology in response to climate change (Rosenzweig et al., 2007) and improve our understanding of the abiotic but also biotic (metabolic and genetic) triggers that determine seasonal changes in plant development. Currently, descriptions of phenology in dynamic vegetation models are poor and need to be improved and tested against long-term field observations if we are to predict the impact of climate change on ecosystem function and CO_2 sequestration (Keenan et al., 2014b; Kucharik et al., 2006; Richardson et al., 2011).

Variations in the concentrations of pigments and spectral properties of leaves also provide a valuable mechanistic link to changes in plant development and photosynthetic rates when interpreted with models such as PROSAIL that combine our knowledge of radiative transfer through forest canopies and leaf mesophyll cells with leaf biochemistry (Jacquemoud and Baret, 1990; Jacquemoud et al., 2009). Automated techniques to detect and assimilate changes in the optical signals of leaves

either near the canopy or remotely from space in conjunction with the coupling of radiative transfer models with biogeochemical models will help to improve the representation of leaf phenology and physiology in dynamic vegetation models (Garrity et al., 2011; Hilker et al., 2011; Klosterman et al., 2014).

This paper aims to synthesise data from flux sites across Europe where researchers have embraced the opportunity to establish automatic observations of phenological events by mounting digital cameras and recording daily (or even hourly) images of the vegetation throughout the seasons. We examine whether coherent seasonal changes in digital image properties can be observed at the majority of sites even if camera types and configuration are not yet harmonised and calibration procedures are not fully developed. In this work our two main objectives were to (1) assess how well digital images can be processed automatically to reveal the key phenological events such as leaf out, flowering, leaf fall, or land management practices such as mowing and harvesting using a piecewise regression approach and; (2) provide a mechanistic link between digital images, leaf phenology and the physiological performance of leaves in the canopy? To address the second question, we adapted the model PROSAIL (Jacquemoud and Baret, 1990; Jacquemoud et al., 2009) to simulate the seasonal changes in red, green and blue signals detected by digital cameras above canopies and performed sensitivity analysis of these signals to variations in canopy structure (leaf area, structure and angles) and biochemistry (leaf pigment and water content).

2 Material and methods

2.1 Study sites and camera set-up

The European network of digital cameras currently covers over 50 flux sites across Europe (Fig. 1 and Table 1). Table 1 demonstrates that a diverse selection of commercially available cameras are being used across the network. The cameras are installed in waterproof housing that is firmly attached to the flux tower some height above the top of the canopy. The cameras are generally orientated North, looking slightly down to the horizon to ensure that the majority of the image contains the vegetation of interest. Canopy images of the same scene are taken repeatedly each day, at a frequency that varies across the different sites from between 1 to 12 images per day and stored as 8-bit JPEG files (i.e. digital numbers ranging from 0 to 255). The archived images used in the present analysis are all taken between 11:00 and 13:00 local time. The camera setup is specific to each camera type but a common requirement to observe the seasonal colour fraction time-series is to set the colour balance to "fixed" mode (on the Stardot cameras) or the white balance to "manual" mode (for the Nikon Coolpix cameras) (Mizunuma et al., 2013; Mizunuma et al., 2014).

[Figure 1 here].

[Table 1 here].

2.2 Image analysis

2.2.1 ROI selection and colour analysis

For each site, a squared region of interest (ROI) was selected from visual inspection of the images. The ROI had to be as large as possible and common to all images of the

same growing season while including as many plants as possible but no soil or sky areas. Image ROIs were then analysed using the open-source image analysis software, Image-J (Image-J v1.36b; NIH, MS, USA). A customised macro was used to extract Red-Green-Blue (RGB) digital number (DN) values between 0 and 255 (n_{colour}) for each pixel of the ROI and a mean value for all pixel values in a given ROI of each image was calculated. Various colour indices can be obtained from digital image properties (Mizunuma et al., 2011), but here we used only the chromatic coordinates, called colour fraction hereafter (Richardson et al., 2007):

$$\text{Colour Fraction} = n_{\text{colour}} / (n_{\text{red}} + n_{\text{green}} + n_{\text{blue}}), \quad (1)$$

where colour is either red, green or blue.

In the following we will thus refer to the "green fraction" as the mean green colour fraction for all pixels in the ROI, as opposed to the amount of pixels covered by vegetation in the entire image (Comar et al., 2012).

2.2.2 Data filtering procedure

Image quality is often adversely affected by rain, snow, low clouds, aerosols, fog and uneven patterns of illumination caused by the presence of scattered clouds. These influences often create noise in the trajectories of colour indices, and is an important source of uncertainty that can hamper the description of canopy seasonal variations and the derivation of robust phenological metrics from colour index time-series. To remove problematic images that were affected by raindrops, snow or fog from the digital photograph analysis, we used a filtering algorithm based on the statistical properties of the time series, we used two steps to filter the raw data. The first filter, based on the deviation from a smoothed spline fit as described in Migliavacca et al.

(2011), was used to remove outliers. Thereafter, we applied the method implemented in Sonnentag et al. (2012), to reduce the variability of the colour fractions (Fig. 2).

[Figure 2 here]

2.2.3 Piecewise break point change analysis

We used a piecewise break point regression approach to extract automatically the main phenological events such as leaf emergence and senescence from the colour fraction time series (Fig. 2). The procedure is implemented in the R package *strucchange* (Zeileis et al., 2002; Zeileis et al., 2003) and is used to detect breaks in a time series by identifying points where the multiple linear correlation coefficients shift from one stable regression relationship to another (Bai and Perron, 2003). The 95% confidence intervals of the identified break points were then computed using the distribution function proposed by Bai (1997). To obtain credible breakpoints in complex green fraction time series such as in highly managed sites (e.g. grazed or cut grasslands, multiple rotation crops) the possibility of identifying numerous peaks or breakpoints (up to 8 breaks) may be necessary. However, such a high number of break points would be excessive in natural ecosystems, and so we decided to set a maximum of five breakpoints per growing season, for both managed and natural ecosystems. We opted for a breakpoint approach over other commonly used methods to extract phenological transitions from time series (i.e thresholds, derivative methods) because it can be considered as more robust and less affected by noise in the time series (Henneken et al., 2013). This is particularly relevant for our application that encompasses a large dataset consisting of many different camera set-ups (camera type, target distance, image processing).

2.2.4 Determining phenophases by visual assessment

In order to relate the break point detection method to phenological phases we also visually examined images from broadleaf forest ecosystems for leafing out, senescence and leaf fall. Six pre-trained observers looked through the same daily images and used a common protocol to identify dates when (1) the majority of vegetation started leafing out (i.e. when 50% of the ROI contains green leaves), (2) the canopy first started to change colour to (first non-green colours such as yellow and orange) in autumn and (3) the last day when a few non-green leaves were still visible on the canopy before the day the branches became bare.

These visually assessed dates were then averaged across observers and compared to the relevant breakpoints identifying the same phenological stage. The leafing out phase was associated to the first automatically detected breakpoint, leaf senescence to the penultimate breakpoint and leaf fall to the last breakpoint. Based on this classification the key dates identified by the algorithm and visual inspection were consistently correlated with one another (Fig. 3). However, there was a tendency for the automatic algorithm to identify all the phenological transitions before the visually assessed dates, by about a week. Also, visual inspections had larger standard deviations, especially during canopy senescence. Because of this systematic difference between the two methods, the breakpoints indicating the start of the growing season were in agreement with visually inspected dates to within 9 days only, and an even lower accuracy was found for leaf senescence and leaf fall (RMSE of 15.9 and 13.3 days respectively). These RMSE values fall, however, within the range recently found by Klosterman et al. (2014) in a similar validation exercise performed with data from various US deciduous forests.

[Figure 3 breakpoint analysis vs visual inspection here]

2.3 Radiative transfer modelling

To interpret mechanistically the colour fraction time-series produced by cameras in the network, we combined the bi-directional radiative transfer model PROSAIL (Jacquemoud and Baret, 1990; Jacquemoud et al., 2009) with some basic spectral properties of the photodetectors and the transmittances of the optical elements and filters used in the cameras, all combined into the so-called spectral efficiency of the RGB color channels (G_{RGB}, in DN W^{-1}, defined as the digital number per watt). This version of PROSAIL has been made available to the research community on the following repository (https://bitbucket.org/jerome_ogee/webcam_network_paper). This version of PROSAIL is required to make the necessary link between the DN values measured by the camera sensors to the reflectances simulated by PROSAIL. It is also necessary to take into account the camera set-up and specific characteristics. Examples of these properties are shown in Supplementary Materials (Figs. S1 and S2) for two types of camera from the network: (1) the Stardot NetCam CS5, in use at the majority of the European sites (Table 1) and the dominant camera used in the North American Phenocam network (http://phenocam.sr.unh.edu/webcam/) (Toomey et al., 2015)and (2) the Nikon Coolpix 4500, in use at two sites within the European camera network, and *ca*. 17 sites within the Japanese Phenological Eyes Network (PEN) (http://pen.agbi.tsukuba.ac.jp/index_e.html) (Nasahara and Nagai, 2015).

The PROSAIL model combines the leaf biochemical model PROSPECT (PROSPECT-5) that simulates the directional-hemispherical reflectance and transmittance of leaves over the solar spectrum from 400 to 2500 nm (Jacquemoud and Baret, 1990) and the radiative-transfer model SAIL (4SAIL (Verhoef, 1984)). The SAIL model assumes that diffusers are randomly distributed in space (turbid medium assumption) and thus may not be applicable for very clumped canopies such as sparse

forests or crops (e.g. vineyards, orchards…). Furthermore, the radiative transfer model assumes only one type of foliage, and therefore cannot deal well with species mixtures. However, for mixed forests, PROSAIL can still be used to interpret RGB signals if the ROI selected on the images is dominated by one single species. The version of the model used here (version 5B for IDL http://teledetection.ipgp.jussieu.fr/prosail/) requires 11 parameters from PROSAIL (leaf area, leaf angle, leaf mass and chlorophyll, carotenoid, water or brown pigment contents, hotspot parameter, leaf structural parameter and dry soil fraction, percentage of diffuse light) as well as geometrical parameters (sun height, view zenith angle and sun-view azimuthal difference angle). The percentage of diffuse light ($\phi_{diffuse}$) is necessary to calculate the amount of direct and diffuse incoming radiation spectra at the top of the canopy and is estimated here from observed incoming global radiation (R_g, in W m^{-2}) using a procedure developed by Reindl *et al*. (1990). The incoming radiation spectra at the top of the canopy are then estimated from R_g, $\phi_{diffuse}$, and mean, normalised spectra for direct (I_{direct}) and diffuse ($I_{diffuse}$) radiation derived by Francois *et al*. (2002) using the 6S atmospheric radiative transfer model (Fig. S3). The 6S simulations performed by François *et al*. considered a variety of aerosol optical thicknesses at 550 nm (corresponding to a visibility ranging from 8.5 to 47.7 km), water vapor content (from 0.5 to 3.5 g cm^{-2}, corresponding to most situations encountered in mid-latitudes), solar incident angle (from 0° to 78.5°) and standard values for ozone, CO_2 and other atmospheric constituents but did not consider the presence of clouds. Therefore the derived spectra are only valid for cloud-free conditions and, following Francois *et al*. (2002), values of $\phi_{diffuse}$ below 0.5 were considered to represent such cloud-free sky conditions. PROSAIL was then used to estimate the amount of light reflected by the canopy in the direction of the camera for

each wavelength $E(\lambda)$ (W m^{-2} nm^{-1}) from which we compute the RGB signals according to:

$$I_{RGB} = B_{RGB} \int_{\lambda_{UV}}^{\lambda_{IR}} G_{RGB}(\lambda) E(\lambda) d\lambda \quad (2)$$

where λ_{UV} and λ_{IR} are the UV and IR cut-off wavelengths of the camera sensor and filter (see Fig. S1) and B_{RGB} is a constant factor that accounts for camera settings (mostly colour balance) and was manually adjusted for each RGB signal and each camera/site using a few days of measurements outside the growing season. The modelled RGB color fractions were then computed in a similar fashion as in Eq. 1 but with I_{RGB} instead of n_{colour}. In practice, G_{RBG} is often normalised to its maximum value rather than expressed in absolute units and for this reason I_{RGB} is not a true digital number, but this has no consequence once expressed in colour fractions. Also, we are aware that the image processing of real (non-uniform) scenes is far more complex than Eq. 2 (Farrell et al., 2012) but from the preliminary results presented below, this simplistic formulation is robust enough to describe time-series of average colour fractions over a large and fixed ROI, measured with different camera settings.

2.4 CO_2 Flux analysis

A recent study by Toomey et al. (2015) demonstrated that the seasonal variability in daily green fraction measured at 18 different flux sites generally correlated well with GPP estimated from co-located flux towers over the season. However, they found that the correlation between daily GPP and daily green fraction was better for some plant functional groups (grasslands) than for others (evergreen needleleaf forests or deciduous broadleaf forests). Thus for some of the flux sites presented in Table 1, we also related qualitatively, changes in vegetation indices to gross primary productivity (GPP) time-series. Net CO_2 fluxes were continuously measured at each site using the

eddy covariance technique described in Aubinet et al., (2012). Level 4 datasets were both quality-checked and gap-filled using online eddy-covariance gap-filling and flux-partitioning tools provided by the European flux database cluster (Lasslop et al., 2010; Reichstein et al., 2005). Full descriptions of the flux tower set-ups used to compare digital images and GPP are provided in Wilkinson et al., (2012) for Alice Holt (deciduous forest), Wohlfahrt et al. (2008) and Galvagno et al. (2013) for Neustift and Torgnon (sub-alpine grasslands), Vesala et al. (2010) for Hyytiälä (evergreen forest) and Aubinet et al. (2009) for Lonzee (cropland).

3 Results and Discussion

3.1 Seasonal changes in green fraction across the network

3.1.1 Needleleaf forest ecosystems

Differences in the seasonal evolution of canopy green fractions are presented for individual years at a selection of needleleaf forest flux sites spanning a latitudinal gradient of approximately *ca*. 30 degrees (31˚20'N - 61˚50'N) (Fig. 4 and Table 1). It was often difficult to automatically determine the start of the growing season for the coniferous sites, either because of snow cover (noticeable changes in the colour signals were often associated with the beginning and end of snow cover) or because of problems caused by the set-up of the camera (either too far away from the crown or containing too much sky). However seasonal changes in the amplitude of the canopy green fraction of needleleaf trees were generally conservative across sites and often displayed a gentle rise in green fraction values during the spring months (Fig. 4a) and a gentle decrease during the winter months. In contrast, the deciduous *Larix* site in

Italy showed a steep and pronounced start and end to the growing season that lasted approximately five months (Fig. 4b).

[Figure 4 Latitude plot for needleleaf forests here]

The main evergreen conifer species *Pinus sylvestris* L. and *Picea abies* L. exhibited different green fraction variations during spring. In *Picea* species, new shoots contain very bright, light green needles that caused a noticeable increase in the green colour fraction during the months of May and June (Fig. 4, e.g. Tharandt and Wetzstein). In contrast, the new shoots of *Pinus* species primarily appeared light brown as the stem of the new shoot elongated (Fig. S4) and caused a small reduction in the green fraction, only detectable at a number of sites and years (Brasschaat in 2009, 2012; Norunda in 2011; Hyytiälä in 2008, 2009, 2010, 2012), followed by an increase in the green fraction values once needle growth dominated at the shoot scale (Fig. 4 and S4). The breakpoint analysis could identify a change in the green fraction when the canopy became consistently snow-free or covered in snow, but also when it experienced sustained daily mean air temperatures of above 0˚C (Fig. 5). For instance, at the Finnish site Hyytiälä, the green fraction exhibited rapid changes during final snowmelt (day 18, bp1) and first snowfall (day 346, bp5 confirmed with visual inspection of the images), but also around days 100-110 (bp2) as daily mean temperatures increased from -10˚C and stabilised for several days just above 0˚C and GPP rates increased (Fig. 5). Towards the end of the growing season significant changes in the green fraction were again detected by the piecewise regression approach, one around day 267 (bp3), coinciding with the period when minimum air temperatures began to fall below 0^{o}C and another around day 323 (bp4) coinciding with a short period of warmer temperatures (Fig. 5). Interestingly from the first breakpoints at the beginning of the year, day 115 (bp2) coincided with the onset of

GPP. Whereas towards the end of the season day 323 (bp4) coincided with a stable period of no photosynthesis (GPP = 0 gC m^{-2} d^{-1}) and a transient increase of daily mean temperature above 0°C. However, the start of this stable period with no photosynthetic uptake was not detected by a breakpoint. During this period the green fraction tracked fluctuations in the daily mean temperature. The recovery of biochemical reactions and the reorganisation of the photosynthetic apparatus in green needles is known to be triggered when air temperature rises above 0˚C (Ensminger et al., 2008; Ensminger et al., 2004) and at about 3-4˚C at this particular site in Finland (Porcar-Castell, 2011; Tanja et al., 2003). Our results suggest that green fractions from digital images seem sensitive enough to detect these changes in the organisation of the photosynthetic apparatus of the coniferous evergreen needles as they acclimate to cold temperatures.

3.1.2 Grassland and cropland ecosystems

Many land surface models still lack crop-related plant functional types and often substitute cropland areas with the characteristics of grasslands (Osborne et al., 2007; Sus et al., 2010). Our initial results from the European phenology camera network demonstrate the difficulty of teasing apart the seasonal and inter-annual developmental patterns as they are often complicated by co-occuring agricultural practices (e.g. cutting, ploughing, harvesting and changes in animal stocking density) (Fig. 6).

[Figure 6 Latitude plot for grasslands and croplands here]

Overall we found that there was surprisingly little difference between the onset dates of growth for most of the permanent grassland sites, despite being located in very different locations across Europe. However the onset of the green fraction signal was considerably delayed at the sub-alpine grassland site in Torgnon compared with the

other sites (Fig. 6). Torgnon also had the most compressed growing season of all the sites, encompassing a period of less than 100 days, some 100 days shorter than the other sites. These differences in growing season length between permanent grassland sites are caused by elevation (most grassland sites are situated at 1000±50 m a.s.l., while the Italian site Torgnon is located at *ca*. 2160 m a.s.l.), that induced differences in temperature and snow cover and consequently the RGB signals.

Management practices such as the cutting of meadows (e.g. Neustift and Früebüel) and changes in animal stocking rate (e.g. Laqueuille) also created abrupt shifts in the RGB signals that could be distinguished from digital images. For example at the Neustift site in Austria, the meadow was cut three times during the 2011 growing season (days 157, 213, 272) causing pronounced drops in the blue fraction and to a lesser extent reductions in the green and red signal (Figs. 7 and S5). These meadow cuts were clearly identified in the green fraction time-series by the breakpoint analysis (see bp3, bp4 and bp5 in Figs. 6, 7 & S5). In addition, flowering events were frequently strong drivers of the colour signals at the Neustift site. The vegetation at Neustift has been classified as Pastinaco-Arrhenatheretum and is characterised by a few dominant grass (*Dactylis glomerata*, *Festuca pratensis*, *Phleum pratensis*, *Trisetum flavescens*) and forb (*Trifolium pratense* and *repens*, *Ranunculus acris*, *Taraxacum officinale*, *Carum carvi*) species. Flowering of these species caused gradual decreases in the red and green signals for several weeks prior to mowing (e.g. the yellow flowers of *R. acris* and *T. officinale* on days 131-156 (bp2), and the white flowers of *C. carvi* between days 176-212 see Fig. S5). In contrast the blue signal tended to increase in strength during flowering periods making the impact of the mowing events dramatic when they occurred (Fig. 7). If the piecewise regression algorithm was set to allow the detection of up to 8 breakpoints at those sites,

flowering events were often identified as well as the mowing events but this made the detection of the start and end dates of the growing season even more challenging using automated algorithms, as manual inspection of each breakpoint would be necessary to identify the dates of first leaf growth and leaf death. For example when 8 breakpoints were observed in grassland ecosystems the first breakpoint was frequently caused by the start of the snow free period, as opposed to the start of growth. Subsequent breakpoints typically indicated the phenology and management of the vegetation, particularly mowing and flowering, and suggest a visual inspection of images may still be necessary to clarify the nature and management causes behind breakpoints in some grassland sites. Thus having the option to detect up to 8 breakpoints or more could be an advantage for ecological studies on the phenology of flowering, pollination and community dynamic responses to environmental changes.

[Figure 7 Neustift here]

In addition, at some sites it was not always easy to discern visually from images when a grassland started its first growth as often fresh shoots are hidden by litter and dead material from the previous year. This particular problem may lead to a slight overestimation of the start date of growth and additionally lead to a potential temporal mismatch between GPP and green-up signals. For example at the subalpine site in Torgnon the green fraction and GPP peaked at the same time of year (bp2), but the onset of the green signal in spring lagged the onset of photosynthesis by about 7-10 days (Fig. 8). Given these results at Neustift, Torgnon and the other sites within the network, grassland green signals can provide additional information on the variations in GPP over the season and between years as suggested by Migliavacca et al., (2011) and more recently Toomey et al., (2015) but an underestimation of the growing season length may also occur using our automatic breakpoint detection approach.

[Figure 8 Torgnon grassland here]

As mentioned above, the use of grassland characteristics to describe the phenology of different crops is common in some land surface models. However, at the same site we can see that the start of the growth period for each different crop varies widely over commonly applied rotations. For example at Lonzee in Belgium we found that for individual crop types such as potato and winter wheat the patterns of the green signal were fairly similar between different years (Fig. 9). However, we could still observe variations between years such as a slightly shorter green period for the potatoes in 2014 relative to 2010 or a slightly later start to the season for winter wheat in 2013 relative to 2011.

[Figure 9 Lonzee rotation time-series here]

As huge areas of Europe are dedicated to the production of crops (326 Mha) and grasslands (151 Mha) (Janssens et al., 2003) and are known to be one of the largest European sources of biospheric CO_2 to the atmosphere at a rate of about 33 TgC y^{-1} (Schulze et al., 2009), it is increasingly important that more field observations of developmental or phenological transitions are obtained to constrain the timing and developmental rate of plants *in situ* and improve model simulations. Our initial results from the European phenology camera network show that digital repeat photography may provide a valuable assimilation dataset in the future for providing useful indicators of developmental transitions and agricultural practices (e.g. cutting, ploughing, harvesting and changes in animal stocking density).

3.1.3 Broadleaf forest ecosystems

Within the European phenology camera network the majority of broadleaf forest sites are deciduous and are identified easily by the seasonal RGB signals they produce. Typically the start of the temperate growing season coincides with a strong increase in

the relative green fraction (Fig 10). Across the network the timing of this spring green-up varies slightly with latitude, usually occurring first in the southern sites and moving North with the British sites starting later than continental sites at similar latitude (for the same years data not shown) (Fig 10). The end of the growing season, identified clearly as a decrease in the green signal, varied considerably across the network. The more continental sites such as the Hainich and Lägeren deciduous forests exhibited the shortest growing season lengths, whilst the oceanic and Mediterranean sites had far longer growing seasons. A high degree of variability in the timing for colour changes is commonly found in autumn across temperate deciduous ecosystems (Archetti et al., 2008) despite the fact that, at least in the case of European tree species, changes in photoperiod and air temperature are usually considered as the main drivers of the colouration of senescent leaves (Delpierre et al., 2009a; Keskitalo et al., 2005; Menzel et al., 2006).

[Figure 10 Broadleaf latitude plot here]

Interestingly, the evergreen broadleaf forests at the Mediterranean sites in Spain and France displayed similar RGB seasonal variations (Fig. 10b). However, the peak in the green fraction values were observed somewhat later in spring compared to those of the deciduous broadleaf sites. These maximum green fraction values are most probably linked to the production of new leaves that typically occurs at this period in Holm Oak (García-Mozo et al., 2007; La Mantia et al., 2003). Interestingly, a strong decrease in the green fraction was observed prior to the peak at the Spanish site, Majadas del Tieter. Similar, patterns in NDVI time-series have been observed around the same period, at the Puechabon site but for different years to the one studied here (2006-2008) (Soudani et al., 2012). This drop in NDVI was explained by the shedding of old leaves coinciding with the period of leaf sprouting in spring. However, on

inspection of the Spanish site photos (Fig. S6) we found that the canopy during this period was covered in conspicuous male catkin-type flowers that appear yellow-brown in the images (Fig. 10). These flowering events are critical for the production of acorns, that randomly alternate between mast and low production years (Vázquez et al., 1990; Espárrago et al., 1992). Thus, in the case of the Spanish site at least, the strong decrease in the green fraction seemed dominated by a male flowering event, in addition to the shedding of old leaves. In the case of the Puechabon site, visual inspection of the photos did not detect a strong flowering event, however, the camera is located slightly further away from the canopy making it difficult to detect flowers easily by eye. However, phenological records maintained at the site indicate that the period between bp2 and bp3 when the green signal slightly decreases, coincides with the start and end of the male flowering period, as well as leaf fall. In contrast, the signal between bp3 and bp4 indicates the period of leaf flushing for this year. Further studies comparing NDVI signals with digital images should allow us to understand better the observed variations in both signals and their link to phenological events such as flowering and litterfall in evergreen broadleaves and how these vary between years in response to climate.

For broadleaf deciduous (and to some extent evergreen) species our breakpoint approach also detected a significant decline in the green fraction a few weeks after leaf emergence and well before leaf senescence (Figs. 2 and 10). This pattern in the green fraction has also been observed for a range of deciduous tree species in Asia and the USA (Hufkens et al., 2012; Ide and Oguma, 2010; Keenan et al., 2014a; Nagai et al., 2011; Saitoh et al., 2012; Sonnentag et al., 2012; Toomey et al., 2015; Yang et al., 2014). In addition, this feature has also been observed at the leaf scale using scanned images of leaves (Keenan et al., 2014a; Yang et al., 2014) and at the

regional scale for a number of deciduous forest sites using MODIS surface reflectance products (Hufkens et al., 2012; Keenan et al., 2014a). The causes that underlie the shape and duration of this large peak at the beginning of the growing season presently remain unclear. Recent camera studies that have also measured either leaf or plant area index at the same time have found no dramatic reductions in leaf area during this rapid decline in the green fraction following budburst (Keenan et al., 2014a; Nagai et al., 2011). At two of the deciduous sites within our network, Alice Holt and Søro (Fig. 10), daily PAR transmittance was also measured providing a suitable proxy for changes in canopy leaf area. In both cases no decrease in the LAI proxy was detected during the decrease of the green signal shortly after budburst. If this decrease in the green signal after leaf growth is not caused by a reduction in the amount of foliage in most cases, it is likely associated with either changes in the concentration and phasing of the different leaf pigments or changes in the leaf angle distribution. These different hypotheses are tested in the next section.

3.2 Modelling ecosystem RGB signals

3.2.1 Sensitivity analysis of model parameters

Using the PROSAIL model as described above, with the camera sensor specifications of the Alice Holt oak site (see Fig. S1) we performed three different sensitivity analyses of the simulated RGB fractions to the 13 model parameters (Table 2). All sensitivity analyses consisted of a Monte Carlo simulation of between 2000 and 10000 runs each. For the first analysis the model was allowed to freely explore different combinations of the parameter space over the range of values commonly found in the literature and with no constraints on how the parameters were related to each other (all parameters being randomly and uniformly distributed). The results

from this initial sensitivity analysis indicated that the RGB signals were sensitive to 4 parameters: the leaf chlorophyll ([Chl]), carotenoid ([Car]) and brown contents (C_{brown}) and the leaf structural parameter (N) (see supplementary material, Fig. S7). In contrast the simulated RGB signals were relatively insensitive to leaf mass (LMA), leaf water content (EWT) and, to some extent, to LAI (above a value of *ca*. 1). This sensitivity analysis also nicely demonstrates how measurements of NDVI made above canopies are most strongly influenced by LAI and to a slightly lesser extent by leaf pigment contents. Recent studies have also discussed whether changes in leaf inclination angle have a strong affect on the green fraction over the growing season (Keenan *et al*., 2014). Our simulations for two different camera view angles (one looking across the canopy and another looking down (results not shown)) indicate that this particular parameter did not have a strong impact on the RGB fractions (Fig. S7).

The model also demonstrated that the impact of diffuse light had a negligible impact on the green fraction. In contrast, an increase in the blue fraction alongside a decrease in the red fraction was observed as the percentage of diffuse light increased (Fig. S7). This result was anticipated given the different spectra prescribed for incoming direct and diffuse light (Fig. S3). However, it is also important to bear in mind that colour signals throughout this manuscript are expressed as relative colour fractions (Eq. 1), and thus strong increases in one or more colour fraction, influenced by strong changes in a particular parameter (e.g. [Chl]….) must also be compensated for by decreases in one or more of the other colour signals.

In a second sensitivity analysis conducted over the same timeframe we refined our assumptions on how certain parameters were likely to vary with one another in spring during the green-up. For this, we fixed all parameters to values typical for English oak during spring conditions (Demarez et al. 1999; Kull et al. 1999), except for LAI and

the concentrations of chlorophyll and carotenoid. We then imposed two further conditions stating that (1) leaf chlorophyll contents increased in proportion to LAI (i.e. the ratio of [Chl]/LAI was normally distributed) and (2) carotenoid and chlorophyll contents also increased proportionally (i.e. [Car]/[Chl] was normally distributed around 30±15%). This ratio between pigment contents is commonly found in temperate tree species. For example, Feret *et al*. (2008, see Fig. 3 therein) showed a strong correlation between the concentrations of chlorophylls a/b and carotenoids for a range of plant types. This second sensitivity analysis revealed clearly how the RGB fractions would likely respond to LAI, chlorophyll and carotenoid contents during the spring green-up (Fig. 11). Firstly, we observed that the RGB signals were more sensitive to LAI, [Chl] and [Car] when the analysis was constrained by our *a priori* conditions (compare panels from Fig. 11 with those of S7). In addition we found that the RGB fractions varied in sensitivity across the range of LAI variations typically found in deciduous forests. Most of the sensitivity in the green signal was found at very low values of LAI (<2), whereafter the signal became insensitive. In contrast, the NDVI signal remained sensitive throughout the full range of prescribed LAI values. For the range of likely [Chl] taken from the literature for oak species (Demarez et al., 1999; Gond et al., 1999; Percival et al., 2008; Sanger, 1971; Yang et al., 2014), our simulations indicated that the sharp increase in the green signals observed by the camera sensors during leaf out are mostly caused by an increase in [Chl]. More interestingly, and contrary to our previous analysis where changes in [Chl] and [Car] were not correlated (compare the same panels in Fig 11 with those presented in Fig. S7), this new analysis clearly shows that, when [Chl] reached *ca*. 30 μg cm^{-2}, the green signal begins to respond negatively to a further increase in [Chl]. This is because in this simulation an increase in [Chl] is accompanied by an increase in

carotenoids and the green fraction responds negatively to an increase in [Car] (Figs. 11 and S7). Another interesting feature of this sensitivity analysis is how the dependence of NDVI on pigment content was greater when we imposed the two constraints described above. This investigation with the PROSAIL model therefore suggests that the sharp reduction in the green fraction commonly observed after budburst in deciduous forests is mostly driven by an increase in leaf pigment concentrations.

[Figure 11 here sensitivity analysis at Alice Holt during spring]

3.2.2 Modelling seasonal RGB patterns mechanistically

Using the PROSAIL model and a few assumptions on how model parameters varied over the season (Table 2, Fig. 12) we investigated the ability of the PROSAIL model to simulate seasonal variations of the RGB signals measured by two different cameras installed at the Alice Holt site. For this a proxy for seasonal variations in LAI was obtained by fitting a relationship to values of LAI estimated from measurements of transmittance as described in Mizunuma et al. (2013), while the expected range and seasonal variations of [Chl], [Car], C_{brown} and N were estimated from several published studies on oak leaves (Demarez et al., 1999; Gond et al., 1999; Percival et al., 2008; Sanger, 1971; Yang et al., 2014), as summarised in Table 2. We also manually adjusted the parameter B_{RGB} in Eq. 4 to match the RGB values measured by the camera during the winter period prior to budburst (highlighted by the grey bar in Fig. 12).

[Figure 12 here seasonal PROSAIL simulations at AliceHolt]

Using this simple model parameterisation, the model was able to capture relatively well the seasonal pattern and absolute magnitude of the three colour signals, including the spring 'green hump' (Fig. 12). As anticipated from our sensitivity analysis

(Fig. 11) we found that at the beginning of the growing season the initial rise in the green signal is dominated by small changes in LAI and [Chl], whilst the small decrease in the green signal that follows is most likely caused by the further increase of [Chl] and [Car]. This period is also characterised by a strong decrease in the red signal and a strong increase in the blue fraction that distinguishes it clearly from the effect of changes in LAI (as blue and green signals remain constant at LAI>2). This relationship is expected as the absorption by chlorophylls and carotenoids are not the same in all wavelengths (Feret *et al*., 2008, see Fig. 8 therein) and can account for most of the observed colour signal trends. Interestingly the maximum green signal observed by the camera coincides with the time when LAI reached half of its maximum value (dotted line on graphs), rather than when [Chl] is maximum. This theoretical result is consistent with pigment concentration data from other recent studies (Keenan et al., 2014a; Yang et al., 2014). Our analysis also indicates that the time when maximum [Chl] and/or [Car] is attained coincides more with the end of the green hump (i.e. several weeks after the peak in the green fraction) and also corresponds to when ecosystem GPP reaches its maximum. Recent pigment concentration measurements performed in the same forest canopy in 2012 and 2013 seem to confirm this theoretical result (data not shown).

Our observations across the deciduous forest sites of the network also highlight a second strong hump in the red and blue signals towards the end of the growing season linked to senescence of the canopy. This autumnal change in colour fractions starts with a decrease in both the green and blue signals and a strong increase in the red signal. To understand this combined signal we conducted a third sensitivity analysis with the model. In this Monte Carlo simulation we maintained all parameters of the model constant except those likely to be important during autumn, mainly LAI, [Chl],

[Car], C_{brown} and N (Table 2). Correlations between [Chl] and LAI on one hand and [Car] and [Chl] on the other hand were kept as for the sensitivity analysis shown in Fig. 11.

The results from this third sensitivity analysis suggest that the start of the autumnal maximum is most likely caused by a reduction in [Chl] and [Car] of the foliage and a simulatenous increase in the structural parameter N and brown pigment concentration (Fig. 12). The degradation of green chlorophyll pigments in autumn has been observed in Oak and other temperate forest species before. Interestingly, the rate of degradation in [Chl] and [Car] during the autumn breakdown is not always proportional and can often lead to a transient increase in the [Car]/[Chl] that allows the yellow carotenoid pigments to remain active as nutrient remobilisation takes place. Leaves of temperate deciduous broadleaf forests in Europe have an overall tendency to yellow in autumn and eventually turn brown before dropping (Archetti, 2009; Lev-Yadun and Holopainen, 2009). This subsequent browning of the foliage is the likely cause for the sharp decrease in the red signal and increase in the blue signal around day 325 (Fig. 12). Visual inspection of the digital images confirmed this was the case and was reflected in the modelling with the increase in C_{brown}, the only parameter that can reconcile the strong reduction in the red signal and the increase in blue strength observed (Fig. 13). Thereafter, reductions in LAI may also contribute further to this trend as leaves fall from the canopy.

[Figure 13 here sensitivity analysis during senescence at AliceHolt]

Results shown in Figs. 11-13 have been done using spectral properties of the Stardot camera, that we obtained directly from the manufacturer (Daniel Lawton, personal communication). However, at Alice Holt both a Stardot camera and a Nikon camera have been operating since 2009 (Mizunuma et al., 2013). Using a similar approach but

with the Nikon camera, we then tested the idea that colour fractions seen by this other camera would also suggest similar variations in leaf pigment and structural parameters over the season. Spectral characteristics of the Nikon Coolpix 4500 were characterised at Hokkaido University in Japan and are shown in the Supplementary material (Fig. S2). We then used these camera specifications and the same parameterisation of canopy structural properties (LAI and N) and leaf pigment concentrations as the those used in Fig. 12. We also manually adjusted B_{RGB} using the same procedure as for the Stardot camera.

From this camera comparison we found that, in order to match the independent RGB camera signals with the same radiative transfer model, only the value of C_{brown} during the growing season had to be adjusted (Fig. S8). On inspection of the camera images this may be justified as the scenes and ROI captured by each camera are very different despite looking at the same canopy, as the Stardot looks across the canopy, whilst the Nikon has a hemi-spherical view looking down on the canopy. Based on the need for different levels of C_{brown}, it is suggested that more brown (woody material) occupies the ROI of the Stardot camera during the vegetation period compared with that in the Nikon image, as confirmed in the images. Besides this difference in C_{brown}, the same model parameterisation reasonably captured the seasonal features of all three colour signals.

3.3 Technical considerations for the camera network

As demonstrated in this paper and elsewhere (Keenan et al., 2014a; Migliavacca et al., 2011), researchers are now exploring the link between canopy colour signals and plant physiology in order to maximise the utility of this relatively inexpensive instrument. However, for this step to proceed further, the network should address several technical considerations.

Firstly, the digital cameras in our European network are currently uncalibrated instruments unlike other commonly used radiometric instruments. In addition, these cameras are deployed in the field and are often exposed to harsh environmental conditions. Thus their characteristics may drift over time. For example although the CMOS sensors (commonly found in the cameras of our network) do not age quickly over periods of several years, the color separation filters on the sensor plate may age after time from UV exposure. Most commercial cameras already contain UV filter protection and in addition they are protectively housed from the elements and sit behind a glass shield that protects the camera from the damage by UV or other environmental conditions, such as water. Also, the studies of Sonnentag *et al*. (2012) and Mizunuma *et al*. (2013; 2014) demonstrated that different camera brands and even different cameras of the same brand that produce different colour fraction time-series reflecting differences in their spectral response still produce coherent phenological metrics. Nonetheless, it would be useful to develop a calibration scheme by digital photography of radiometrically characterised colour sheets such as those used to detect the health and nutritional status of plants (Mizunuma et al., 2014) whilst the camera is in the field and exposed to a variety of light conditions. However, the deployment of such a colour checker for long-term continuous monitoring is problematic as the spectral quality of the colour checker will alter over time as particles, such as dust and insects, accumulate on its surface. An alternative solution could involve routinely checking for sensor drift using images taken during the winter months of different years. For example, at least in the case of deciduous broadleaf species, one or two months before the beginning of the growing season (see grey bar in Fig. 12), the RGB signals tend to display relatively constant values. Provided the camera does not move and the colour balance settings are not changed, this period

could be used to detect problems with the camera when compared over several years. At Alice Holt where two cameras have been operating for at least 5 years we have found no evidence for such drift using winter time values (data not shown). Ideally, it would be desirable to use only digital cameras from manufacturers that provide information on the spectral characteristics of the sensors, filters and algorithms used, or to measure routinely the spectral response of individual cameras within the network as the cameras age.

Secondly, digital camera studies have typically focussed on using the green fraction to deduce the dates of canopy green-up and senescence. The green fraction has been preferred because its signal-to-noise ratio is higher in vegetated ecosystems. For this very reason, and because of inter-pixel dependencies caused by the cameras built-in image processing, we recommend setting the camera up so that the images do not contain too much sky, ideally less than 20%. In addition, as demonstrated in this study, combining the information of all three colour signals may provide more useful information on canopy physiology, phenology and management impacts. However, to look at these particular signals we must understand the effects of other environmental factors that can impact the day-to-day variability of the RGB colour fractions. In particular, colour signals are sensitive to the spectral properties of the incoming light and thus to the percentage of diffuse radiation. Using the PROSAIL model we explored the impact of diffuse radiation on the RGB signals at the Alice Holt site and found that the red and blue fractions were much more affected by rapid changes in sky conditions than the green fraction. When simulating the impact of diffuse light on the RGB response we make use of direct and diffuse light spectra presented in Fig. S3. From the spectra shown in Fig. S3 it is clear that increases in diffuse light will result in more energy received in the blue wavelengths and less energy in the red, thereby

influencing directly the red and blue fractions. This is why there is very little change in the green fraction over the range of diffuse light (%). Furthermore, by incorporating the day-to-day variations in diffuse radiation at the site the model did not reproduce better the red and blue fractions, even for cloud-free conditions (Fig. 14), demonstrating that the influence of diffuse light was not easy to account for in the model. This can be problematic as the percentage of diffuse light, unlike other variables such as leaf area index or pigment concentrations, can change dramatically from one day to the next. For this reason, the green fraction is probably the best suited signal for detecting rapid changes in leaf area and pigment concentrations, at least within their lower range of values (0-2 for LAI and 0-30μg cm^{-2} for [Chl]). However, these results will need to be checked thoroughly for the different cameras across the entire network.

[Figure 14 here model-data comparison at AliceHolt for NC cloud-free]

Lastly, cameras within the network are so far not thermally regulated. Our preliminary results using the two most commonly used cameras in the networks (Stardot and Nikon Coolpix) seem to indicate that images are not sensitive to contrasting temperatures. This point will certainly need to be addressed more thoroughly in future studies and could be addressed by taking black images periodically to assess the level of instrument noise and it's relationship with temperature. If this could be achieved then it would be possible to at least reduce noise in the signals caused by temperature.

4 Conclusions

This synthesis analysis of the European camera network demonstrates that using digital repeat photography at a daily resolution can aid the automatic identification of

inter-annual variations in climate–driven vegetation status such as the emergence of new foliage (i.e. bud burst, regrowth), flowering, fruit development, leaf senescence and leaf abscission. Furthermore, agricultural practices are captured well by the camera providing a useful archive of images and colour signal changes that can be interrogated with complementary flux datasets. In the long term such datasets collected across the different networks of flux sites will become invaluable for investigating in detail the connections between climate and growing season length, and will contribute to a better understanding of the underlying controls on plant development and how these vary between plant functional types, species and location. Currently, large-scale estimates of photosynthesis are principally derived from models with highly uncertain parameterisations. In particular, large-scale vegetation models have difficulties predicting when the growing season starts and ends (Richardson *et al.*, 2011), how this relates to the carbon uptake period and the magnitude of photosynthetic rates attained during peak summertime. Traditionally, the remote sensing NDVI products are generally used for linking large-scale variations of vegetation phenology and terrestrial primary productivity to climate change (Running *et al.*, 2004, Zhou *et al.*, 2003). However the spatial resolution of such measurements is typically low (>100m) and the temporal resolution often inhibitive for tracking the dynamic transitions of canopy cover over a mosaic of heterogeneous land surfaces leading to problems reconstructing robustly the seasonal changes in canopy cover (Hagolle *et al.*, 2010, Quaife & Lewis, 2010).

Our results indicate that by combining variations in the Red, Green and Blue (RGB) colour fractions and mechanistic radiative transfer models, these digital archives can be used to quantify changes in the plants' physiological status and constrain estimates

of NDVI (see Fig. S7). Thus near-surface measurements could provide RGB ground-truth estimates for similar remotely-sensed multi-spectral satellite products (Hufkens *et al.*, 2012a) and provide the link between remotely sensed products and ecosystem physiology measured at flux towers (Migliavacca *et al.*, 2011, Richardson *et al.*, 2007, Wingate *et al.*, 2008; Mizunuma et al., 2013). This technological breakthrough will provide a means of increasing our understanding of how canopy pigment contents vary between ecosystems and with climate and improve predictions of the CO_2 sequestration period and potential of terrestrial ecosystems at large scales.

Acknowledgments

Lisa Wingate was supported through a CarboEurope-IP grant awarded to Professor John Grace (University of Edinburgh), a Marie Curie Intra-European Fellowship (LATIS) awarded to L.Wingate and a NERC Advanced Research Fellowship awarded to L.Wingate. Salary for Toshie Mizinuma and the equipping of several sites within the European network with cameras was kindly supported through a Jim Gray Seed Trust Award from Microsoft Research awarded to L.Wingate. Edoardo Cremonese acknowledges financial support from the PhenoALP project, an Interreg project co-funded by the European Regional Development Fund, under the operational program for territorial cooperation Italy-France (ALCOTRA) 2007–2013. The Alice Holt site is funded by the UK Forestry Commission, and the StarDot camera installation was funded through the Life+ FutMon project (LIFE07 ENV/D/000218) of the European Commission. Manuela Balzarola acknowledges financial support from the EU-project Geoland2. Andreas Ibrom received funding by the Danish strategic research project ECOCLIM and the EU project CARBO-extreme, whilst installation of the webcam was initiated and funded by the EU infrastructure project IMECC. We also kindly acknowledge fieldwork funding from the British Embassy Tokyo and the British Council UK-Japan 2008 collaborative Project Grant Award, GHG Europe and STSM support for T.Mizunuma from the EUROSPEC Cost Action ES0903. We also thank the Phenological Eyes Network and the US Phenocam Network and especially Andrew Richardson and Shin Nagai for their assistance and encouragement developing the European network. We are also grateful to Daniel Lawton for his fast response time to questions regarding the technical details for the Stardot camera. Finally, we are sincerely grateful to the ongoing support of the European Flux

1 database team and the FLUXNET research community for their continuous co-
2 operation, assistance and participation in the activities of the camera network.
3

References

Ahrends H.A., Etzold S., Kutsch W., Stoeckli R., Bruegger R., Jeanneret F., Wanner H., Buchmann N., Eugster W. (2009) Tree phenology and carbon dioxide fluxes: use of digital photography for process-based interpretation at the ecosystem scale. Climate Research 39:261-274.

Aono Y., Kazui K. (2008) Phenological data series of cherry tree flowering in Kyoto, Japan, and its application to reconstruction of springtime temperatures since the 9th century. International Journal of Climatology 28:905-914.

Archetti M. (2009) Phylogenetic analysis reveals a scattered distribution of autumn colours. Annals of Botany 103:703-713.

Archetti M., Doring T.F., Hagen S.B., Hughes N.M., Leather S.R., Lee D.W., Lev-Yadun S., Manetas Y., Ougham H.J., Schaberg P.G., Thomas H. (2008) Unravelling the evolution of autumn colours: an interdisciplinary approach. TREES 24:166-173.

Aubinet M., Vesala T., Papale D. (2012) (Ed.)^(Eds.) Eddy Covariance: A Practical Guide to Measurement and Data Analysis, Springer Atmospheric Sciences. Netherlands

Aubinet M., Moureaux C., Bodson B., Dufranne D., Heinesch B., Suleau M., Vancutsem F., Vilret A. (2009) Carbon sequestration by a crop over a 4-year sugar beet/winter wheat/seed potato/winter wheat rotation cycle. Agricultural and Forest Meteorology 149:407-418. DOI: 10.1016/j.agrformet.2008.09.003.

Bai J. (1997) Estimation of a change point in multiple regression models. Review of Economics and statistics. 79:551-563.

Bai J., Perron P. (2003) Computation and analysis of multiple structural change models. Journal of Applied Econometrics 18:1-22.

Baldocchi D. (2014) Measuring fluxes of trace gases and energy between ecosystems and the atmosphere - the state and future of the eddy covariabce method. Global Change Biology 20:3600-3609. DOI: 10.1111/gcb.12649.

Baldocchi D.D., Falge E., Gu L., Olson R., Hollinger D., Running S., Anthoni P., Bernhofer C. (2001) FLUXNET: a new tool to study the temporal and spatial variability of ecosystem-scale carbon dioxide, water vapor, and energy flux densities. Bulletin of American Meteorological Society 82:2415-2434.

Baldocchi D.D., Black T.A., Curtis P.S., Falge E., Fuentes J.D., Granier A., Gu L., Knohl A., Pilegaard K., Schmid H.P., Valentini R., Wilson K., Wofsy S., Xu L., Yamamoto S. (2005) Predicting the onset of net carbon uptake by deciduous forests with soil temperature and climate data: a synthesis of FLUXNET data. International Journal of Biometeorology 49:377-387.

Beer C., Reichstein M., Tomelleri E., Ciais P., Jung M., Carvalhais N., Rödenbeck C., Altaf Arain M., Baldocchi D., Bonan G.B., Bondeau A., Cescatti A., Lasslop G., Lindroth A., Lomas M., Luyssaert S., Margolis H., Oleson K.W., Roupsard O., Veenendaal E., Viovy N., Williams C., Woodward F.I., Papale D. (2010) Terrestrial gross carbon dioxide uptake: global distribution and covariation with climate. Science 329:834-838.

Ciais P., Reichstein M., Viovy N., Granier A., Ogée J., Allard V., Aubinet M., Buchmann N., Bernhofer C., Carrara A., Chevalier F., de Noblet N., Friend A., Friedlingstein P., Grünwald T., Heinesch B., Keronen P., Knohl A., Krinner G., Loustau D., Manca G., Matteucci G., Miglietta F., Ourcival J.-M., Papale D., Pilegaard K., Rambal S., Seufert G., Soussana J.-F., Sanz M.J.,

Schulze E.-D., Vesala T., Valentini R. (2005) Europe-wide reduction in primary productivity caused by the heat and drought in 2003. Nature 437:529-533.

Comar A., Burger P., de Solan B., Baret F., Daumard F., Hanocq J.-F. (2012) A semi-automatic system for high throughput phenotyping wheat cultivars in-field conditions: description and first results. Functional Plant Biology 39:914-924.

Delpierre N., Dufrene E., Soudani K., Ulrich E., Cecchini S., Boe J., Francois C. (2009a) Modelling interannual and spatial variability of leaf senescence for three deciduous tree species in France. Agricultural and forest meteorology 149:938-948.

Delpierre N., Soudani K., François C., Köstner B., Pontailler J.-Y., Nikinmaa E., Misson L., Aubinet M., Bernhofer C., Granier A., Grünwald T., Heinesch B., Longdoz B., Ourcival J.-M., Rambal S., Vesala T., Dufrêne E. (2009b) Exceptional carbon uptake in European forests during the warm spring of 2007: a data-model analysis. Global Change Biology 15:1455-1474.

Demarée G.R., Rutishauser T. (2009) Origins of the Word "Phenology"". EOS Trans. AGU, 90 (34):291. DOI:10.1029/2009E0340004

Demarez V., Gastellu-Etchegorry J.P., Mougin E., Marty G., Proisy C., Dufrêne E., Le Dantec V. (1999) Seasonal variation of leaf chlorophyll content of a temperate forest. Inversion of the PROSPECT model. International Journal of Remote Sensing 20:879-894.

Ensminger I., Schmidt L., Lloyd J. (2008) Soil temperature and intermittant frost modulate the rate of recovery of photosynthesis in Scots pine under simulated spring conditions. New Phytologist 177:428-442.

Ensminger I., Sveshnikov D., Campbell D.A., Funk C., Jansson S., Lloyd J., Shibistova O., Oquist G. (2004) Intermittant low temperatures constrain spring recovery of photosynthesis in boreal Scots pine forests. Global Change Biology 10:995-1008.

Farrell J., Catrysse P.B., Wandell B. (2012) Digital camera simulation. Applied Optics 51:A80-A90.

Francois C., Ottlé C., Olioso A., Prévot L., Bruguier N., Ducros Y. (2002) Conversion of 400–1100 nm vegetation albedo measurements into total shortwave broadband albedo using a canopy radiative transfer model. Agronomie 22, 611-618:doi:10.1051/agro:2002033.

Friend A.D., Arneth A., Kiang N.Y., Lomas M., Ogee J., Rodenbeck C., Running S.W., Santaren J.-D., Sitch S., Viovy N., Ian Woodward F., Zaehle S. (2007) FLUXNET and modelling the global carbon cycle. Global Change Biology 13:610-633. DOI: doi:10.1111/j.1365-2486.2006.01223.x.

Galvagno M., Wohlfahrt G., Cremonese E., Rossini M., Colombo R., Filippa G., Migliavacca M. (2013) Phenology and carbon dioxide source/sink strength of a subalpine grassland in response to an exceptionally short snow season. Environmental Research Letters 8:25008 DOI:10.1088/1748-9326/8/2/025008

García-Mozo H., Gómez-Casero M.T., Domínguez E., Galán C. (2007) Influence of pollen emission and weather-related factors on variations in holm-oak (*Quercus ilex* subsp. *ballota*) acorn production. Environmental and Experimental Botany 61:35-40.

Garrity S.R., Bohrer G., Maurer K.D., Mueller K.L., Vogel C.S., Curtis P.S. (2011) A comparison of multiple phenology data sources for estimating seasonal transitions in deciduous forest carbon exchange. Agricultural and Forest Meteorology 151:1741-1752.

Gond V., De Pury D.G.G., Veroustraete F., Ceulemans R. (1999) Seasonal variations in leaf area index, leaf chlorophyll, and water content; scaling-up to estimate fAPAR and carbon balance in a multilayer, multispecies temperate forest. Tree Physiology 19:673-679.

Hagolle O, Huc M, Villa Pascual D, Dedieu G (2010) A multi-temporal method for cloud detection, applied to FORMOSAT-2, VENμS, LANDSAT and SENTINEL-2 images. *Remote Sensing of Environment,* **114**, 1747-1755.

Henneken R., Dose V., Schleip C. & Menzel A. (2013) Detecting plant seasonality from webcams using Bayesian multiple change point analysis. Agr. For. Met. 168:177-185.

Hilker T., Gitelson A., Coops N.C., Hall F.G., Black T.A. (2011) Tracking plant physiological properties from multi-angular tower-based remote sensing. Oecologia, 165 (4), 865-876 doi: 10.1007/s00442-010-1901-0.

Hufkens K., Friedl M., Sonnentag O., Braswell B.H., Milliman T., Richardson A.D. (2012) Linking near-surface and satellite remote sensing measurements of deciduous broadleaf forest phenology. Remote Sensing of Environment 117:307-321.

Ide R., Oguma H. (2010) Use of digital cameras for phenological observations. Ecological Informatics 5:339-347.

Jacquemoud S., Baret F. (1990) PROSPECT: A model of leaf optical properties spectra. Remote Sensing of Environment 34:75-91.

Jacquemoud S., Verhoef W., Baret F., Bacour C., Zarco-Tejada P.J., Asner G.P., Francois C., Ustin S.L. (2009) PROSPECT+SAIL models: A review of use for vegetation characterization. Remote Sensing of Environment 113:556-566.

Janssens I.A., Freibauer A., Ciais P., Smith P., Nabuurs G.-J., Folberth G., Schlamadinger B., Hutjes R.W.A., Ceulemans R., Schulze E.D., Valentini R., Dolman A.J. (2003) Europe's Terrestrial Biosphere Absorbs 7 to 12% of European Anthropogenic CO_2 Emissions. Science 300:1538-1542.

Janssens I.A., Lankreijer H., Matteucci G., Kowalski A.S., Buchmann N., Epron D., Pilegaard K., Kutsch W., Longdoz B., Grünwald T., Montagnani L., Dore S., Rebmann C., Moors E.J., Grelle A., Rannik Ü., Morgenstern K., Oltchev S., Clement R., Gudmundsson J., Minerbi S., Berbigier P., Ibrom A., Moncrieff J., Aubinet M., Bernhofer C., Jensen N.-O., Vesala T., Granier A., Schulze E.-D., Lindroth A., Dolman A.J., Jarvis P.G., Ceulemans R., Valentini R. (2001) Productivity overshadows temperature in determining soil and ecosystem respiration across European forests. Global Change Biology 7:269-278.

Jung M., Reichstein, M., Ciais, P., Seneviratne, S. I., Sheffield, J., Goulden, M. L., Bonan, G., Cescatti, A., Chen, J., de Jeu, R., Dolman, A.J., Eugster, W., Gerten, D., Gianelle, D., Gobron, N., Heinke, J., Kimball, J., Law, B.E., Montagnani, L., Mu, Q., Mueller, B., Oleson, K., Papale, D., Richardson, A. D., Roupsard, O., Running, S., Tomelleri, E., Viovy, N., Weber, U., Williams, C., Wood, E., Zaehle, S., and Zhang, K.: Recent decline in the global land evapotranspiration trend due to limited moisture supply, Nature, 467, 951–954, 2010.

Keeling C.D., Chin J.F.S., Whorf T.P. (1996) Increased activity of northern vegetation inferred from atmospheric CO2 measurements. Nature 382:146-149.

Keenan T.F., Darby B., Felts E., Sonnentag O., Friedl M., Hufkens K., O'Keefe J., Klosterman S., Munger J.W., Toomey M., Richardson A.D. (2014a) Tracking forest phenology and seasonal physiology using digital repeat photography: a

critical assessment. Ecol. Appl., 24, 1478–1489, doi:10.1890/13-0652.1, 2014a.
Keenan T.F., Gray J., Friedl M.A., Toomey M., Bohrer G., Hollinger D.Y., Munger J.W., O'Keefe J., Schmid H.P., Wing I.S., Yang B., Richardson A.D. (2014b) Net carbon uptake has increased through warming-induced changes in temperate forest phenology. Nature Climate Change, 4, 598-604 DOI: 10.1038/NCLIMATE2253.
Keskitalo J., Bergquist G., Gardestrom P., Jansson S. (2005) A cellular timetable of autumn senescence. Plant Physiology 139:1635-1648.
Kljun N., Black, T. A., Griffis, T. J., Barr, A. G., Gaumont-Guay, D., Morgenstern, K., McCaughey, J.H., and Nesic, Z.: . (2006) Response of net ecosystem productivity of three boreal forest stands to drought. Ecosystems 9:1128-1144.
Klosterman S.T., Hufkens K., Gray J.M., Melaas E., Sonnentag O., Lavine I., Mitchell L., Norman R., Friedl M.A., Richardson A.D. (2014) Evaluating remote sensing of deciduous forest phenology at multiple spatial scales using PhenoCam imagery. Biogeosciences 11:4305-4320. DOI: doi:10.5194/bg-11-4305-2014.
Kowalski A.S., Loustau D., Berbigier P., Manca G., Tedeschi V., Borghetti M., Valentini R., Kolari P., Berninger F., Rannik U., Hari P., Rayment M., Mencuccini M., Moncrieff J., Grace J. (2004) Paired comparisons of carbon exchange between undisturbed and regenerating stands in four managed forests in Europe. Global Change Biology 10:1707-1723. DOI: doi:10.1111/j.1365-2486.2004.00846.x.
Krinner G., Viovy N., Noblet-Ducoudré N.d., Ogée J., Polcher J., Friedlingstein P., Ciais P., Sitch S., Prentice I.C. (2005) A dynamic global vegetation model for studies of the coupled atmosphere-biosphere system. Global Biogeochemical Cycles 19:GB1015, doi:10.1029/2003GB002199.
Kucharik C.J., Barford C.C., El Maayar M., Wofsy S.C., Monson R.K., Baldocchi D. (2006) A multiyear evaluation of a Dynamic Global Vegetation Model at three AmeriFlux forest sites: Vegetation structure, phenology, soil temperature, and CO_2 and H_2O vapor exchange. Ecological Modelling 196:1-31.
Kutsch W.L., Aubinet M., Buchmann N., Smith P., Osborne B., Eugster W., Wattenbach M., Schrumpf M., Schulze E.D., Tomelleri E., Ceschia E., Bernhofer C., Béziat P., Carrara A., Tommasi P.D., Grünwald T., Jones M., Magliulo V., Marloie O., Moureaux C., Olioso A., Sanz M.J., Saunders M., Søgaard H., Ziegler W. (2010) The net biome production of full crop rotations in Europe. Agriculture, Ecosystems and Environment 139:336-345.
La Mantia T., Cullotta S., Garfi G. (2003) Phenology and growth of *Quercus ilex* L. in different environmental conditions in Sicily (Italy). Ecologia mediterranea 29:15-25.
Lasslop G., Reichstein M., Papale D., Richardson A.D., Arneth A., Barr A.G., Stoy P., Wohlfahrt G. (2010) Separation of net ecosystem exchange into assimilation and respiration using a light response curve approach: critical issues and global evaluation. Global Change Biology 16:187-208.
Lawrence D.M., Slingo J.M. (2004) An annual cycle of vegetation in a GCM. Part I: Implementation and impact on evaporation, . Climate Dynamics 22:87–105.
Le Maire G., Delpierre N., Jung M., Ciais P., Reichstein M., Viovy N., Granier A., Ibrom A., Kolari P., Longdoz B., Moors E.J., Pilegaard K., Rambal S., Richardson A.D., Vesala T. (2010) Detecting the critical periods that underpin

interannual fluctuations in the carbon balance of European forests. J. Geophys. Res., 115, G00H03, doi:10.1029/2009JG001244, 2010.
Lev-Yadun S., Holopainen J.K. (2009) Why red-dominated autumn leaves in America and yellow-dominated autumn leaves in Northern Europe? New Phytologist 183:497-501.
Linkosalo T., Hakkinen R., Terhivuo J., Tuomenvirta H., Hari P. (2009) The time series of flowering and leaf bud burst of boreal trees (1846–2005) support the direct temperature observations of climatic warming. Agricultural and forest meteorology 149:453-461.
Magnani F., Mencuccini M., Borghetti M., Berbigier P., Berninger F., Delzon S., Grelle A., Hari P., Jarvis P.G., Kolari P., Kowalski A.S., Lankreijer H., Law B.E., Lindroth A., Loustau D., Manca G., Moncrieff J.B., Rayment M., Tedeschi V., Valentini R., Grace J. (2007) The human footprint in the carbon cycle of temperate and boreal forests. Nature 447:849-851.
Menzel A., Sparks T.H., Estrella N., Koch E., Aasa A., Ahas R., Alm-Kubler K., Bissolli P., Braslavska O.G., Briede A., Chmielewski F.M., Crepinsek Z., Curnel Y., Dahl A., Defila C., Donnelly A., Filella Y., Jatczak K., Mage F., Mestre A., Nordli O., Penuelas J., Pirinen P., Remisova V., Scheifinger H., Striz M., Susnik A., Van Vliet A.J.H., Wielgolaski F.-E., Zach S., Zust A.N.A. (2006) European phenological response to climate change matches the warming pattern. Global Change Biology 12:1969-1976. DOI: doi:10.1111/j.1365-2486.2006.01193.x.
Migliavacca M., Galvagno M., Cremonese E., Rossini M., Meroni M., Cogliati S., Manca G., Diotri F., Busetto L., Colombo R., Fava F., Pari E., Siniscalco C., Morra di Cella U., Richardson A.D. (2011) Using digital repeat photography and eddy covariance data to model grassland phenology and photosynthetic CO_2 uptake. Agricultural and forest meteorology 151:1325-1337.
Mizunuma T., Koyanagi T., Mencuccini M., Nasahara K.N., Wingate L., Grace J. (2011) The comparison of several colour indices for the photographic recording of canopy phenology of Fagus crenata Blume in eastern Japan. . Plant Ecology and Diversity, 4, 67-77.
Mizunuma T., Wilkinson M., Eaton E.L., Mencuccini M., Morison J.I.L., Grace J. (2013) The relationship between carbon dioxide uptake and canopy colour from two camera systems in a deciduous forest in southern England. Functional Ecology 27:196-207.
Mizunuma T., Mencuccini M., Wingate L., Ogée J., Nichol C., Grace J. (2014) Sensitivity of colour indices for discriminating leaf colours from digital photographs. Methods in Ecology and Evolution. 5, 1078–1085, doi:10.1111/2041-210X.12260, 2014.
Nagai S., Maeda T., Gamo M., Muraoka H., Suzuki R., Nasahara K.N. (2011) Using digital camera images to detect canopy condition of deciduous broad-leaved trees. Plant Ecology and Diversity 4:79-89.
Nasahara K.N., Nagai S. (2015) Development of an in situ observation network for terrestrial ecological remote sensing: the Phenological Eyes Network (PEN). Ecological Research 30:211-223.
Osborne B., Saunders M., Walmsley D., Jones M., Smith P. (2010) Key questions and uncertainties greenhouse gas balance . Agriculture, Ecosystems and Environment 139:293–301.

Osborne T.M., Lawrence D.M., Challinor A.J., Slingo J.M., Wheeler T.R. (2007) Development and assessment of a coupled crop-climate model. Global Change Biology 13:169-183.

Percival G.C., Keary I.P., Noviss K. (2008) The potential of a chlorophyll content SPAD meter to quantify nutrient stress in foliar tissue of Sycamore (*Acer pseudoplatanus*), English Oak (*Quercus robur*), and European Beech (*Fagus sylvatica*). Arboriculture & Urban Forestry 34:89-100.

Piao S., Ciais P., Friedlingstein P., Peylin P., Reichstein M., Luyssaert S., Margolis H., Fang J., Barr A., Chen A., Grelle A., Hollinger D.Y., Laurila T., Lindroth A., Richardson A.D., Vesala T. (2008) Net carbon dioxide losses of northern ecosystems in response to autumn warming. Nature 451:49-52.

Porcar-Castell A. (2011) A high-resolution portrait of the annual dynamics of photochemical and non-photochemical quenching in needles of *Pinus sylvestris*. Physiologia Plantarum 143:139-153.

Quaife T, Lewis P (2010) Temporal constraints on linear BRDF model parameters. *IEEE Transactions on Geoscience and Remote Sensing,* **48**, 2445-2450.

Reichstein M., Falge E., Baldocchi D., Papale D., Aubinet M., Berbigier P., Bernhofer C., Buchmann N., Gilmanov T., Granier A., Grunwald T., Havrankova K., Ilvesniemi H., Janous D., Knohl A., Laurila T., Lohila A., Loustau D., Matteucci G., Meyers T., Miglietta F., Ourcival J.-M., Pumpanen J., Rambal S., Rotenberg E., Sanz M., Tenhunen J., Seufert G., Vaccari F., Vesala T., Yakir D., Valentini R. (2005) On the separation of net ecosystem exchange into assimilation and ecosystem respiration: review and improved algorithm. Global Change Biology 11:1424-1439.

Reindl D.T., Beckman W.A., Duffie J.A. (1990) Diffues fraction correlations. Solar Energy 45:1-7.

Richardson A.D., Jenkins J.P., Braswell B.H., Hollinger D.Y., Ollinger S.V., Smith M.-L. (2007) Use of digital webcam images to track spring green-up in a deciduous broadleaf forest. Oecologia 152:323-334.

Richardson A.D., Anderson R.S., Altaf Arain M., Barr A.G., Bohrer G., Chen G., Chen J.M., Ciais P., Davis K.J., Desai A.R., Dietze M.C., Dragoni D., Garrity S.R., Gough C.M., Grant R., Hollinger D.Y., Margolis H.A., McCaughey H., Migliavacca M., Monson R.K., Munger J.W., Poulter B., Raczka B.M., Ricciuto D.M., Sahoo A.K., Schaefer K., Tian H., Vargas R., Verbeeck H., Xiao J., Xue Y. (2011) Terrestrial biosphere models need better representation of vegetation phenology: results from the North American Carbon Program Site Synthesis. Global Change Biology 18, 566–584, doi:10.1111/j.1365-20 2486.2011.02562.x, 2012.

Rosenzweig C., Casassa G., Karoly D.J., Imeson A., Liu C., Menzel A., Rawlins S., Root T.L., Seguin B., Tryjanowski P. (2007) Assessment of observed changes and responses in natural and managed systems. , in: M. L. Parry, et al. (Eds.), Climate Change 2007: Impacts, Adaptation and Vulnerability, Contribution of Working Group II to the Fourth Assessment Report of the Intergovernmental Panel on Climate Change, , Cambridge University

Press, , Cambridge, UK,. pp. 79-131.

Saitoh T.M., Nagai S., Saigusa N., Kobayashi H., Suzuki R., Nasahara K.N., Muraoka H. (2012) Assessing the use of camera-based indices for characterizing canopy phenology in relation to gross primary production in a deciduous broad-leaved and an evergreen coniferous forest in Japan. . Ecological Informatics 11:45-54.

Sanger J.E. (1971) Quantitative investigations of leaf pigments from their inception in buds through autumn coloration to decomposition in falling leaves. Ecology 52:1075-1089.

Schulze E.-D., Luyssaert, S., Ciais, P., Freibauer, A., Janssens, I. A., Soussana, J. F., Smith, P., Grace, J., Levin, I., Thiruchittampalam, B., Heimann, M., Dolman, A. J., Valentini, R., Bousquet, P., Peylin ,P., Peters, W., Rodenbeck, C., Etiope, G., Vuichard, N., Wattenbach, M., Nabuurs, G. J., Poussi, Z., Nieschulze, J., Gash, J. H., and the CarboEurope Team: Importance of methane and nitrous oxide for Europe's terrestrial greenhouse-gas balance, Nat. Geosci., 2, 842–850, 2009.

Sonnentag O., Hufkens K., Teshera-Sterne C., Young A.M., Friedl M., Braswell B.H., Milliman T., O'Keefe J., Richardson A.D. (2012) Digital repeat photography for phenological research in forest ecosystems. Agricultural and forest meteorology 152:159-177.

Soudani K., Hmimina G., Delpierre N., Pontailler J.-Y., Aubinet M., Bonal D., Caquet B., de Grandcourt A., Burban B., Flechard C., Guyon D., Granier A., Gross P., Heinesh B., Longdoz B., Loustau D., Moureaux C., Ourcival J.-M., Rambal S., Saint André L., Dufrêne E. (2012) Ground-based Network of NDVI measurements for tracking temporal dynamics of canopy structure and vegetation phenology in different biomes. Remote Sensing of Environment 123:234-245.

Soussana J., Allard, V., Pilegaard, K., Ambus, P., Amman, C., Campbell, C., Ceschia, E., Clifton-Brown, J., Czobel, S., Domingues, R., Flechard, C., Fuhrer, J., Hensen, A., Horvath, L., Jones, M., Kasper, G., Martin, C., Nagy, Z., Neftel, A., Raschi, A., Baronti, S., Rees, R. M., Skiba, U., Stefani, P., Manca, G., Sutton, M., Tuba, Z., and Valentini, R.: Full accounting of the greenhouse gas (CO2 , N2 O, CH4) budget of nine European grassland sites, Agr. Ecosyst. Environ., 121, 121–134, 2007.

Sus O., Williams M., Bernhofer C., Beziat P., Buchmann N., Ceschia E., Doherty R., Eugster W., Grunwald T., Kutsch W., Smith P., Wattenbach M. (2010) A linked carbon cycle and crop developmental model: Description and evaluation against measurements of carbon fluxes and carbon stocks at several European agricultural sites. Agriculture, Ecosystems and Environment 139:402-418.

Tanja S., Berninger F., Vesala T., Markkanen T., Hari P., Makela A., Ilvesniemi H., Nikinmaa E., Huttula T., Laurila T., Aurela M., Grelle A., Lindroth A., Arneth A., Shibistova O., Lloyd J. (2003) Air temperature triggers the recovery of evergreen boreal forest photosynthesis in spring. Global Change Biology 9:1410-1426.

Toomey M., Friedl M., Frolking S., Hufkens K., Klosterman S., Sonnentag O., Baldocchi D., Bernacchi C., Biraud S.C., Bohrer G., Brzostek E., Burns S.P., Coursolle C., Hollinger D.Y., Margolis H.A., McCaughey H., Monson R.K., Munger J.W., Pallardy S., Phillips R.P., Torn M.S., Wharton S., Zeri M., Richardson A.D. (2015) Greenness indices from digital cameras predict the timing and seasonal dynamics of canopy-scale photosynthesis. Ecological Applications 25:99-115.

Valentini R., Matteucci G., Dolman A.J., Schulze E.-D., Rebmann C., Moors E.J., Granier A., Gross P., Jensen N.O., Pilegaard K., Lindroth A., Grelle A., Bernhofer C., Grünwald T., Aubinet M., Ceulemans R., Kowalski A.S., Vesala T., Rannik Ü., Berbigier P., Loustau D., Guõmundsson J., Thogeirsson

H., Ibrom A., Morgenstern K., Clement R., Moncrieff J., Montagnani L., Minerbi S., Jarvis P.G. (2000) Respiration as the main determinant of carbon balance in European forests. Nature 404:861-865.

Verhoef W. (1984) Light scattering by leaf layers with application to canopy reflectance modeling: the SAIL model. . Remote Sensing of Environment 16:125-141.

Vesala T., Launiainen S., Kolari P., Pumpanen J., Sevanto S., Hari P., Nikinmaa E., Kaski P., Mannila H., Ukkonen E., Piao S.L., Ciais P. (2010) Autumn temperature and carbon balance of a boreal Scots pine forest in Southern Finland. Biogeosciences 7:163-176.

Wilkinson M., Eaton E.L., & B.M.S.J., J.I.L. M. (2012) Inter-annual variation of carbon uptake by a plantation oak woodland in south-eastern England. . Biogeosciences 9:5373-5389.

Wingate L., Richardson A.D., Weltzin J.F., Nasahara K.N., Grace J. (2008) Keeping an eye on the carbon balance: linking canopy development and net ecosystem exchange using a webcam. Fluxletter 1:14-17.

Wohlfahrt G., Hammerle A., Haslwanter A., Bahn M., Tappeiner U., Cernusca A. (2008) Seasonal and inter-annual variability of the net ecosystem CO2 exchange of a temperate mountain grassland: Effects of weather and management. Journal of Geophysical Research 113, D8. DOI: doi:10.1029/2007JD009286.

Wu C., Chen J.M., Gonsamo A., Price D.T., Black T.A., Kurz W.A. (2012) Interannual variability of net carbon exchange is related to the lag between the end-dates of net carbon uptake and photosynthesis: Evidence from long records at two contrasting forest stands. Agricultural and forest meteorology 164:29-38.

Yang X., Tang J., Mustard J. (2014) Beyond leaf color: comparing camera-based phenological metrics with leaf biochemical, biophysical and spectral propoerties throughout the growing season of a temperate deciduous forest. Journal of Geophysical Research Biogeosciences 119, 181–191, doi:10.1002/2013JG002460, 2014.

Zeileis A., Leisch F., Hornik K., Kleiber C. (2002) *strucchange*: An R Package for Testing for Structural Change in Linear Regression Models. . Journal of Statistical Software 7:1-38.

Zeileis A., Kleiber C., Kraemer W., Hornik K. (2003) Testing and dating of structural changes in practice. Computational Statistics and Data Analysis 44:109-123.

Table 1. List of participating sites in the European phenology camera network, period of camera operation, dominant vegetation cover and camera model.

Site	Country	Period	ID	Latitude/Longitude	Dominant ssp.	Camera Model
Evergreen forests (20 sites)						
[1]Värriö	Finland	2008-2015	FI-Var	67˚46'N, 29˚35'E	Scots pine	Canon G1
[2]Nimtek	Sweden	2011-2015	SE-Nim	65˚58'N, 18˚32'E	Spruce/Scots pine	Mobotix M24M
[3]Svartberget (ICOS)	Sweden	2015	SE-Sva	64˚10'N, 19˚47'E	Scots pine/spruce	Stardot Netcam SC5
[4]Hyytiälä (ICOS)	Finland	2008-2015	FI-Hyy	61˚50'N, 24˚17'E	Scots pine	Canon G1
[5]Norunda (ICOS)	Sweden	2009-2015	SE-Nor	60˚05'N, 17˚28'E	Scots pine/spruce	Stardot Netcam SC3
[6]Norunda Clearcut	Sweden	2010- 2015	SE-Nor_cc	60˚05'N, 17˚28'E	Clearcut	2 Mobotix M24M
[7]Skogaryd	Sweden	2013-2015	SE-Sko_cc	58˚22'N, 12˚08'E	Clearcut	Mobotix M24M
[8]Aberfeldy	Scotland	2009	UK_Gri	56˚36'N, 03˚47'W	Sitka spruce	Canon EOS 300D
[9]Rumperöd	Sweden	2013-2015	SE-Rum	56˚19'N, 14˚06'E	Mixed forest	Mobotix M24M
[10]Hyltemossa (ICOS)	Sweden	2015	SE-Hyl	56˚06'N, 13˚25'E	Norway spruce	Stardot Netcam SC5
[11]Brasschaat	Belgium	2009-2015	BE-Bra	51˚18'N, 04˚31'E	Scots pine	Axis 207W
[12]Tharandt	Germany	2009-2015	DE-Tha	50˚58'N, 13˚34'E	Norway spruce	Canon PowerShot S50
[13]Wetzstein	Germany	2008-2015	DE-Wet	50˚27'N, 11˚27'E	Norway spruce	Kodak DC290
[14]Vielsalm	Belgium	2010-2015	BE-Vie	50˚18'N, 05˚59'E	Scots pine	Stardot Netcam SC5
[15]Bilý Kríž	Czechoslovakia	2015	CZ-Bk	49˚30'N, 18˚32'E	Norway Spruce	Canon PowerShot A800
[16]Davos	Switzerland	2012-2015	CH-Dav	46˚49'N, 09˚51'E	Norway spruce	Stardot Netcam SC5
[17]Salles	France	2014-2015	FR-Bil	44˚44'N, 00˚46'W	Maritime pine	Stardot Netcam SC5

[20]Yatir	Israel	2012-2015	IL-Yat	31˚20'N, 35˚3'E	Aleppo pine	Stardot Netcam SC5
Deciduous forests (15 sites)						
[21]Abisko	Sweden	2011-2015	SE-Abi	68˚36'N, 18˚80'E	Birch	Nikon D300s
[22]Sorø	Denmark	2009-2015	DK-Sor	55˚29'N, 11˚38'E	Beech	Stardot Netcam SC5
[23]Hohes Holz	Germany	2014-2015	DE-Hhf	52˚05'N, 11˚13'E	Mixed forest	Stardot Netcam SC5
[24]Alice Holt	UK	2009-2015	UK-Ham	51˚07'N, 00˚51'W	Pedunculate oak	Nikon Coolpix + Stardot NetCam
[25]Wytham Woods	UK	2011-2015	UK-WW	51˚46'N, 01˚20'W	Pedunculate oak	Motobix
[26]Hainich	Germany	2003-2015	DE-Hai	51˚04'N, 10˚28'E	Beech/Ash	Kodak DC290
[27]Vielsalm	Belgium	2010-2015	BE-Vie	50˚18'N, 05˚59'E	Beech	Stardot Netcam SC5
[28]Lanžhot	Czechoslovakia	2014-2015	CZ-Lan	48˚41'N, 16˚57'E	Mixed forest	Campbell ScientificCC5MPX
[29]Hesse	France	2012-2015	FR-Hes	48˚40'N, 07˚03'E	Beech	Stardot Netcam SC5
[30]Montiers	France	2012-2015	FR-Mon	48˚32'N, 05˚18'E	Beech	Stardot Netcam SC5
[31]Fontainebleau	France	2012-2015	FR-Fon	48˚28'N, 02˚46'E	Sessile oak	Axis P1348
[32]Lägeren	Switzerland	2004-2015	CH-Lae	47˚28'N, 08˚21'E	Beech/ash	Stardot Netcam SC5+Nikon Coolpix 5400
[33]Torgnon	Italy	2010-2015	IT-Tor	45˚50'N, 07˚34'E	Larch	Nikon D500
[34]Roccarespampani	Italy	2008-2013	IT-Ro2	42˚39'N, 11˚51'E	oak	Stardot Netcam SC5
[35]Herdade Machoqueira	Portugal	2010-2015	PT_Co1	38˚32'N, 08˚0'W	oak	Stardot Netcam SC5
Grasslands/Croplands (8 and 7 sites)						
[36]Lanna (ICOS)	Sweden	2015	SE-Lan	58˚21'N, 13˚06'E	Cropland	Stardot Netcam SC5
[37]Cabauw	Netherlands	2010-2015	NL-Ca1	52˚01'N, 05˚04'E	Grassland	N/A
[38]Grosses Bruch	Germany	2013-2015	DE-	52˚01'N, 11˚06'E	Grassland	Canon PowerShot D20
[39]Gebesee	Germany	2008-2015	DE-Geb	51˚06'N, 10˚54'E	Cropland	Mobotix M22M (+ Kodak DC290)

[40]Grillenburg	Germany	2007-2015	DE-Gri	50˚57'N, 13˚31'E	Grassland	Canon PowerShot S50
[41]Klingenberg	Germany	2008-2015	DE-Kli	50˚54'N, 13˚31'E	Cropland	Canon PowerShot S50
[42]Lonzee	Belgium	2009-2015	BE-Lon	50˚55'N, 04˚44'E	Cropland	Stardot Netcam SC5
[43]Grignon	France	2005-2015	FR-Gri	48˚50'N, 01˚57'E	Cropland	Logitech webcam Abus 5 MPixel
[44]Neustift	Austria	2011-2015	AT-Neu	47˚06'N, 11˚19'E	Grassland	Logitech webcam
[45]Früebüel	Switzerland	2008-2015	CH-Fru	47˚07'N, 08˚32'E	Grassland	Stardot Netcam SC5
[46]Lusignan	France	2013-2015	FR-Lus	46˚25'N, 00˚07'E	Grassland	Stardot Netcam SC5
[47]Torgnon	Italy	2009-2015	IT-Tor	45˚50'N, 07˚34'E	Grassland	Nikon D500
[48]Laqueuille	France	2010-2015	FR-Lq1	45˚38'N, 02˚44'E	Grassland	Stardot Netcam SC5
[49]Auradé	France	2013-2015	FR-Aur	43˚32'N, 01˚06'E	Cropland	Aote-Tech 5 MegaPixel IP
[50]Lamasquère	France	2013-2015	FR-Lam	43˚29'N, 01˚14'E	Cropland	Aote-Tech 5 MegaPixel IP
Peatlands (6 sites)						
[51]Stordalen (ICOS)	Sweden	2015	SE-Sto	68°21'N, 19°03'E	Peatland	Stardot Netcam SC5
[52]Degerö Stormyr	Sweden	2011-2015	SE-Deg	64°11'N, 19°33'E	Peatland	Canon A480 & Canon A810 & StardotSC5
[53] Siikaneva	Finland	2014-2015	FI-Sii	61°49'N, 24°11'E	Peatland	Canon A810
[54] Fäjemyr	Sweden	2014-2015	SE-Fäj	56°15'N, 13°33'W	Peatland	Canon A810
[55] Auchencorth	UK	2014-2015	UK-AMo	55°47'N, 3°14'W	Peatland	Canon A810
[56]Glencar	Ireland	2013-2015	IR-Gle	51°55'N, 9°55'W	Peatland	Canon A810

1

2

Table 2. List of parameters and values used to model the RGB signals at Alice Holt for the 2010 growing season. Camera-specific parameters for the Stardot Netcam SC5 (NC) and the Nikon Coolpix (ADFC) are given separately.

Parameter	Definition	Value	Reference
$\phi_{diffuse}$	Percentage of diffuse light	25% or calculated (see text)	Reindl *et al*. (1990)
θ_{view}	View zenith angle	10° (ADFC) or 80° (NC)	This study
θ_{sun}	Solar zenith angle	Calculated or 30° (sensitivity analysis)	This study
B_{RGB}	Colour balance	0.92/0.75/1 (ADFC) or 1/0.66/0.73 (NC)	This study
$\phi_{hotspot}$	Hotspot parameter	0.05	Jacquemoud *et al*. (2009)
$\phi_{drysoil}$	Dry soil fraction	0.2	Jacquemoud *et al*. (2009)
φ_{leaf}	Leaf inclination angle	30°	Kull *et al*. (1999)
LMA	Leaf mass per area	80 g m^{-2}	Demarez *et al*. (1999)
LWT	Leaf water thickness	0.04 cm	Demarez *et al*. (1999)
LAI	Leaf area index	See Fig. 12	This study
N	Leaf structural parameter	See Fig. 12	Demarez *et al*. (1999)
[Chl]	Leaf chlorophyll content	See Fig. 12	Demarez *et al*. (1999)
[Car]	Leaf carotenoïd content	See Fig. 12	Demarez *et al*. (1999)
C_{brown}	Leaf brown pigment content	See Fig. 12	Jacquemoud *et al*. (2009)

Figure 1

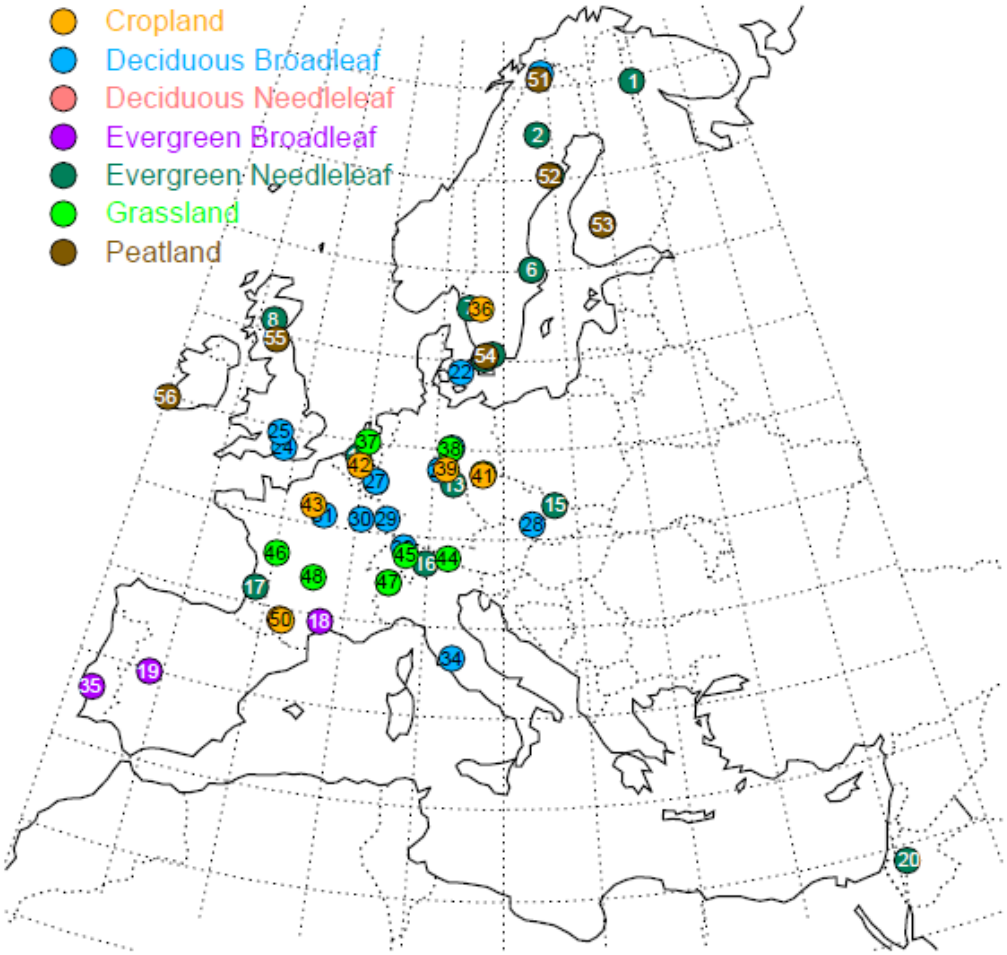

Figure 1. Distribution of operational digital cameras at flux sites across Europe for further details refer to Table 1.

Figure 2

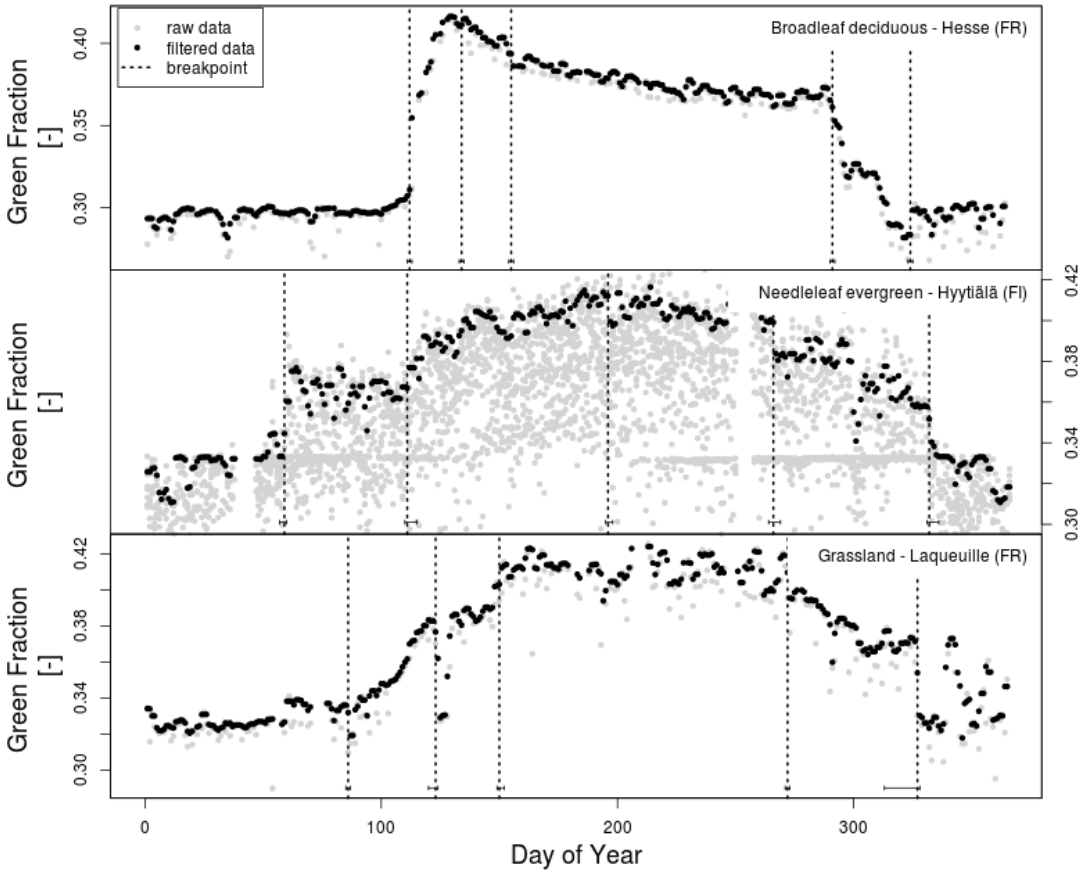

Figure 2. Green fraction time-series for the broadleaf deciduous forest, Hesse in France, the needleleaf evergreen forest Hyytiälä in Finland and the grassland Laqueuille in France, demonstrating the filtering and phenostage extraction approach used in our synthesis. Grey and black dots indicate raw and filtered data, respectively while dashed vertical lines indicate the breakpoints extracted on the green fraction time-series using the piecewise regression approach. At the bottom of each vertical line the 95% confidence interval of the breakpoint dates is also shown.

Figure 3

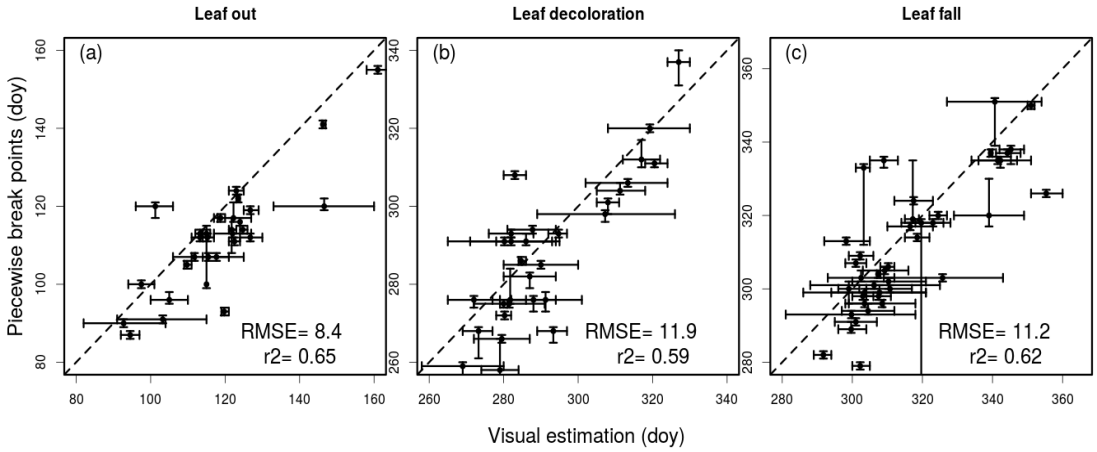

Figure 3. Relationship between the visual estimations of (a) leaf unfolding (b) leaf senescence and (c) leaf fall day number compared to the breakpoint day numbers estimated by the piecewise regression of green colour fractions for the broadleaf sites. Error bars represent the 95% confidence interval, calculated from the mean of observation replicates (n=6) for the visual estimation, and from the error of the piecewise regression coefficients for the breakpoint analysis.

Figure 4

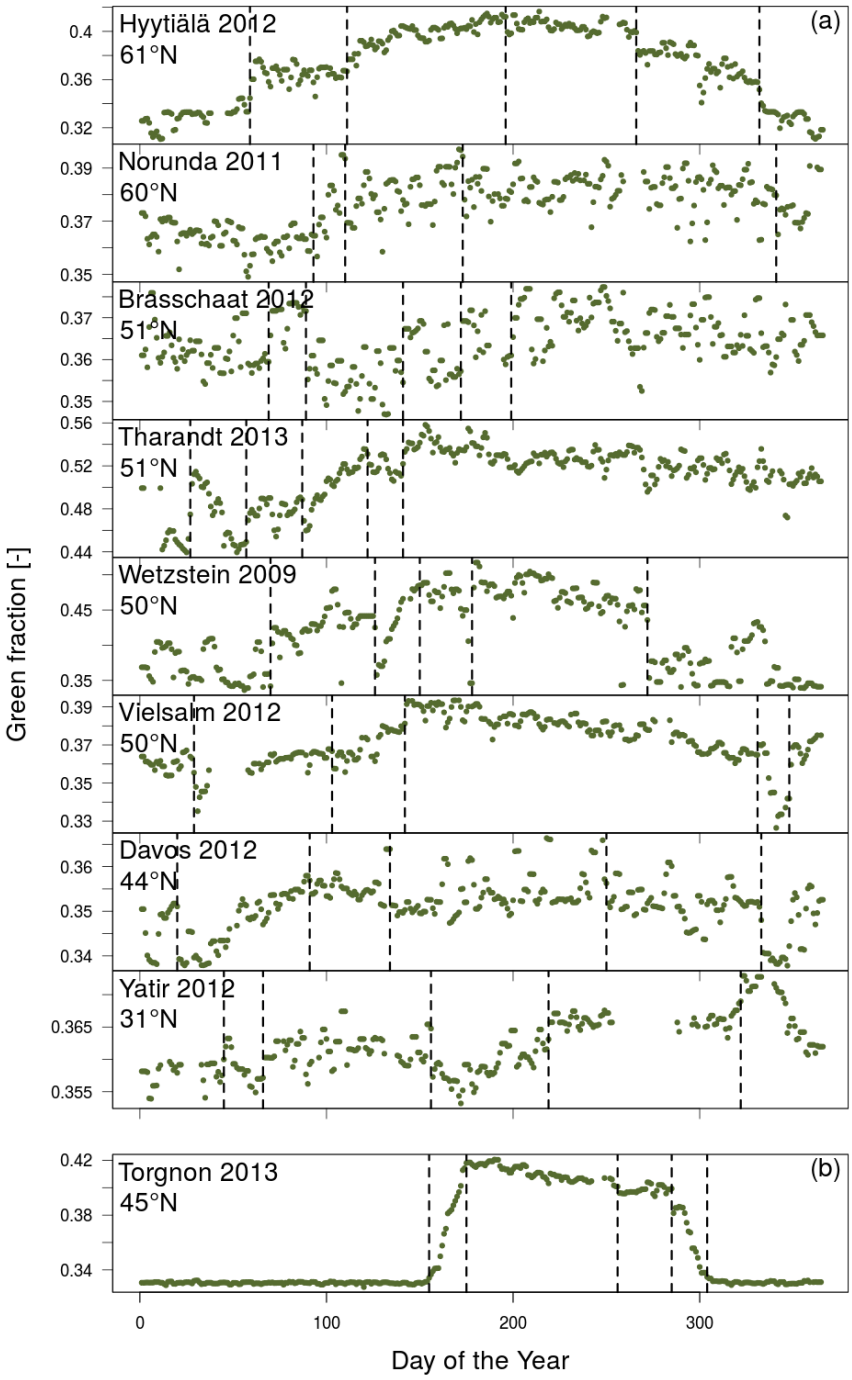

Figure 4. A latitudinal comparison of filtered green fraction time-series for a selection of (a) evergreen and (b) deciduous needleleaf flux sites within the European phenology camera network. Vertical dashed lines indicate breakpoints that correspond to transitions in the green fraction over the growing season.

Figure 5

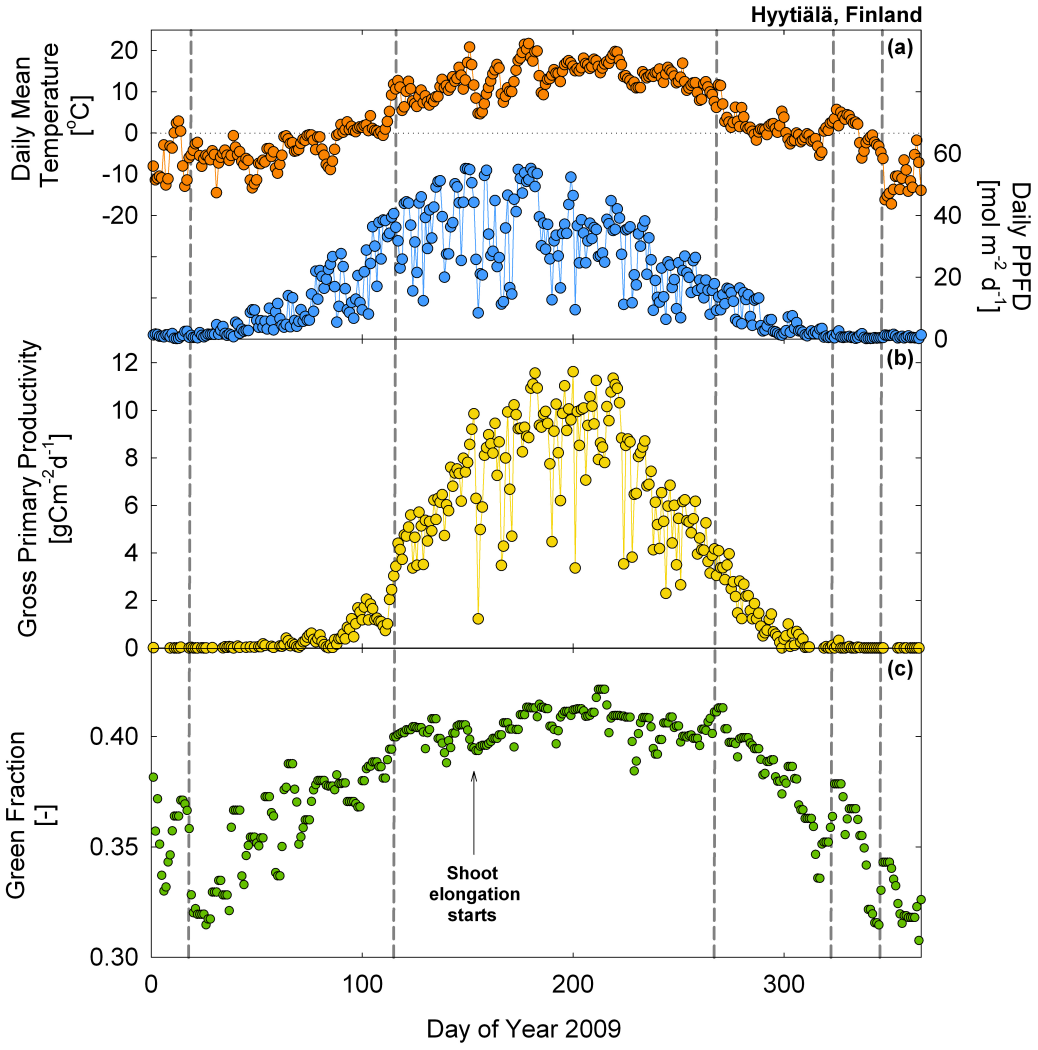

Figure 5. Time-series of (a) daily temperature, daily PPFD (b) GPP (c) green fraction variations over the year with vertical solid lines showing major breakpoint changes identifying important transitions in the green fraction over the growing season at the Hyytiälä flux site in Finland during 2009.

Figure 6

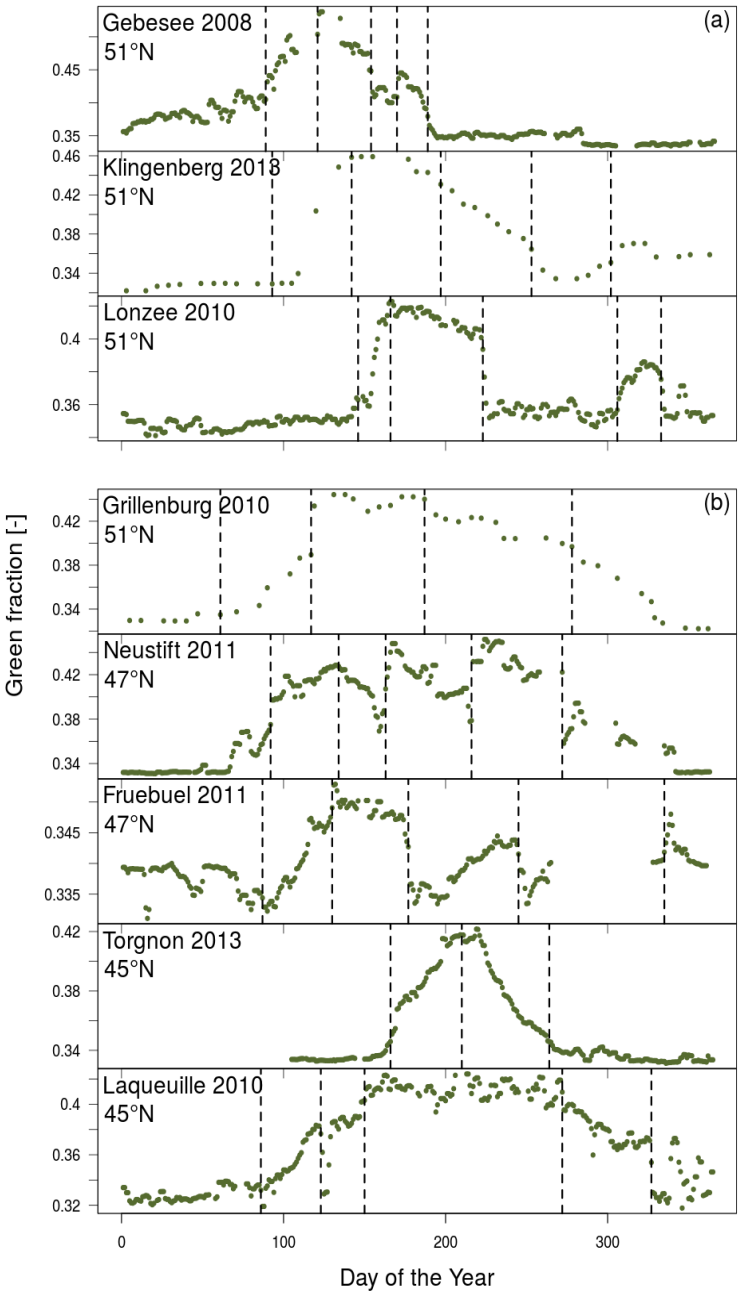

Figure 6. A latitudinal comparison of filtered green fraction time-series for a selection of (a) cropland and (b) grassland flux sites within the European phenology camera network. Vertical dashed lines indicate breakpoints that correspond to transitions in the green fraction over the growing season.

Figure 7

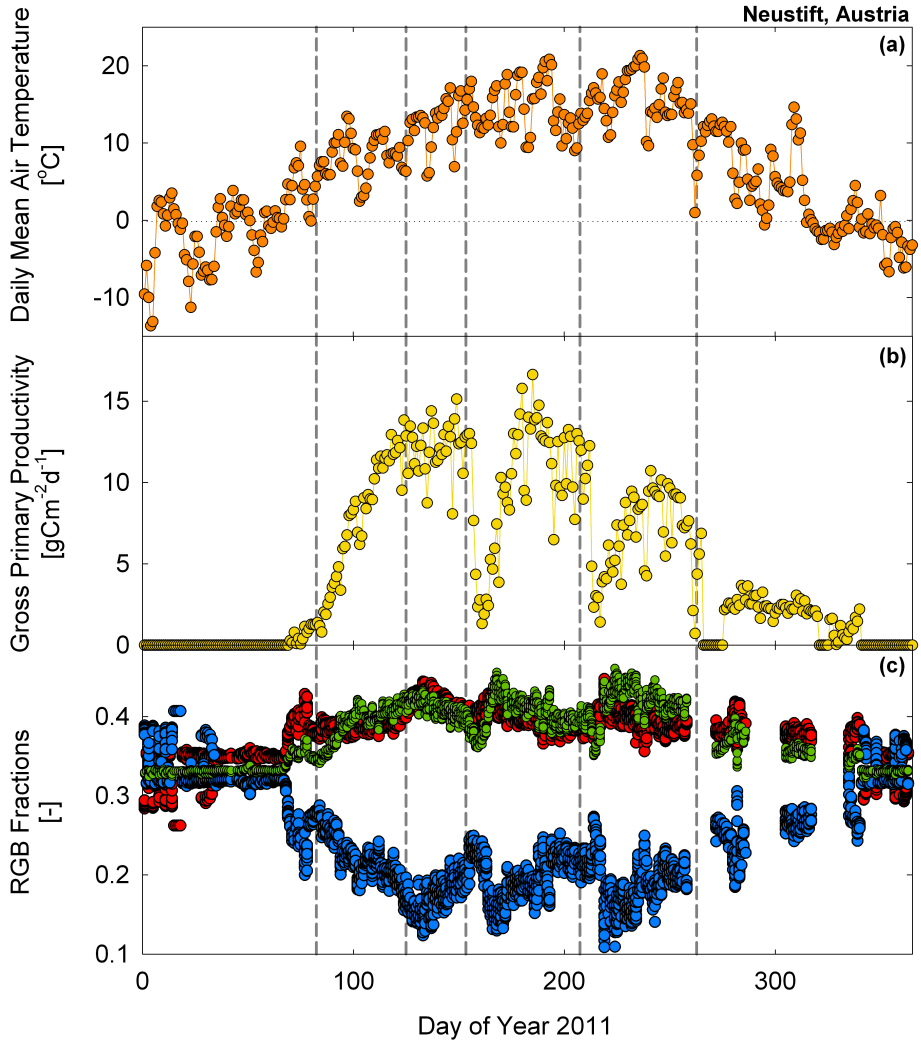

Figure 7. Impact of (a) temperature, phenology and mowing practices on (b) GPP and (c) RGB colour fractions with solid vertical lines showing major breakpoint changes identifying important transitions in the green fraction over the growing season for the alpine meadow flux site Neustift in Austria.

Figure 8

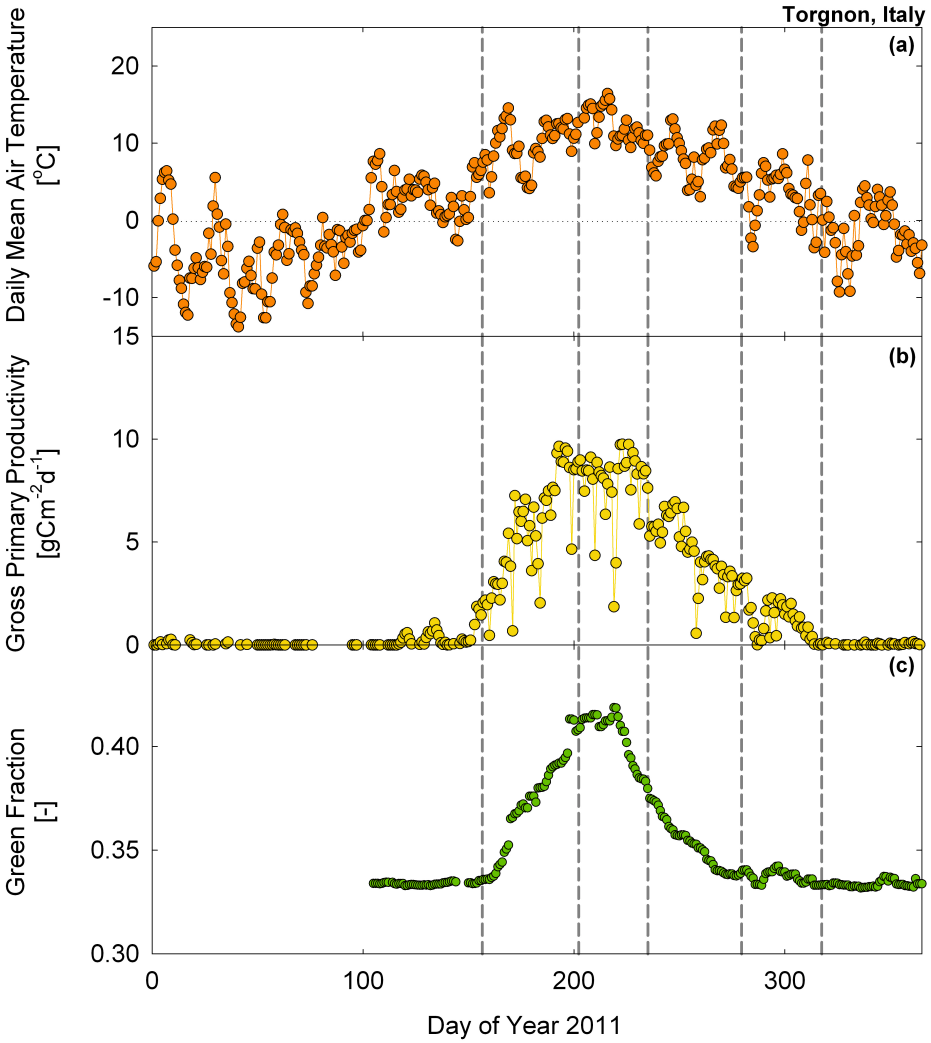

Figure 8. Time-series for the alpine grassland, Torgnon in Italy demonstrating (a) the daily mean air temperature (b) the gross primary productivity and (c) the calculated breakpoints for the green fraction using the piecewise regression approach. Vertical solid lines show major breakpoint changes identifying important transitions in the green fraction over the growing season

Figure 9

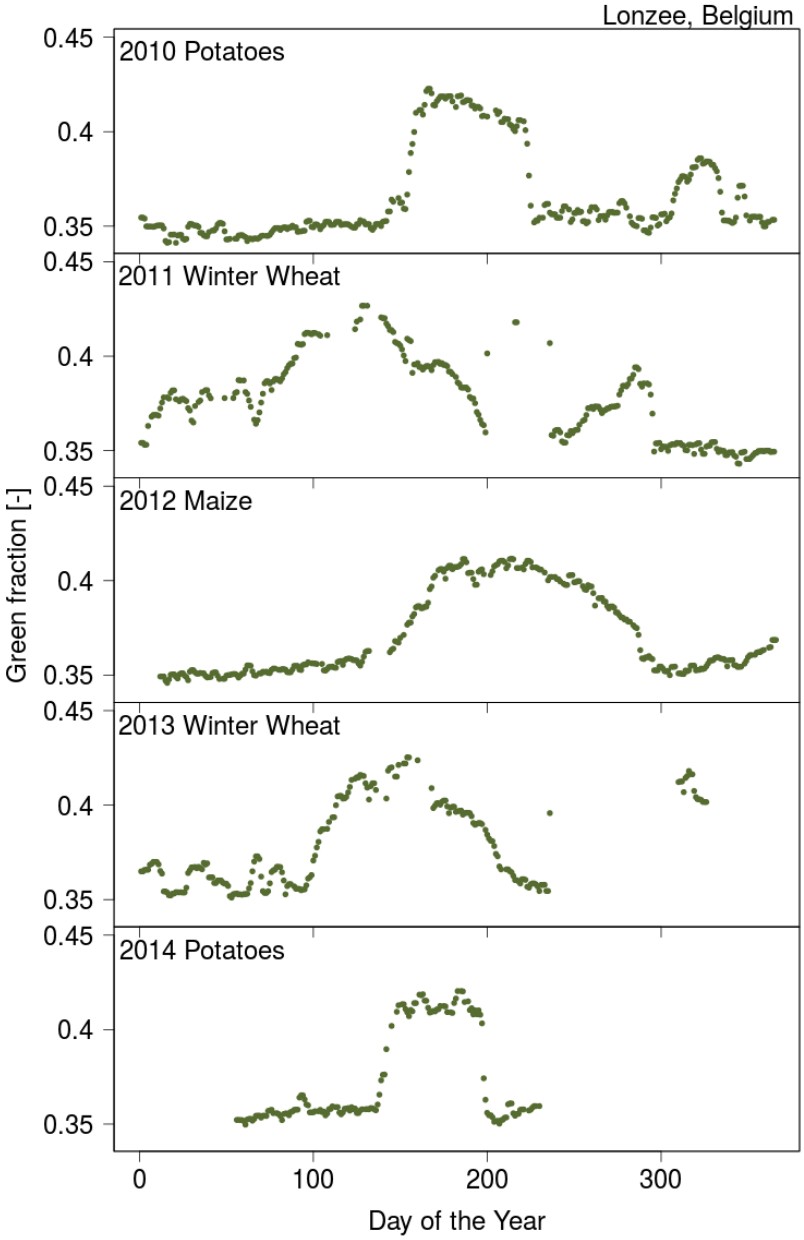

Figure 9. Impact of crop management practices and crop rotation on the green colour fractions over the growing seasons 2010-2014 for the agricultural flux site Lonzee in Germany.

Figure 10

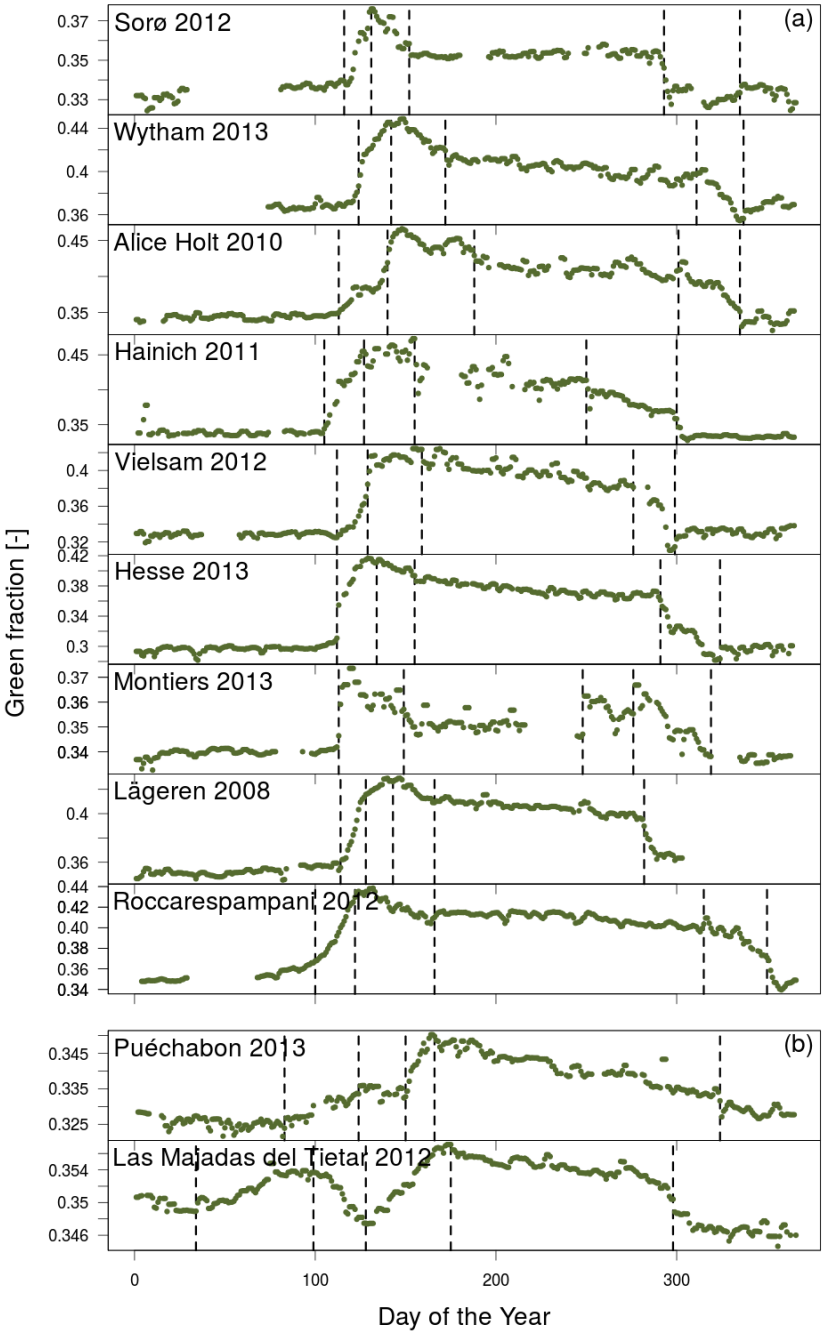

Figure 10. A latitudinal comparison of filtered green fraction time-series for a selection of (a) deciduous and (b) evergreen broadleaf forest flux sites within the European phenology camera network. Vertical dashed lines indicate breakpoints that correspond to transitions in the green fraction over the growing season.

Figure 11

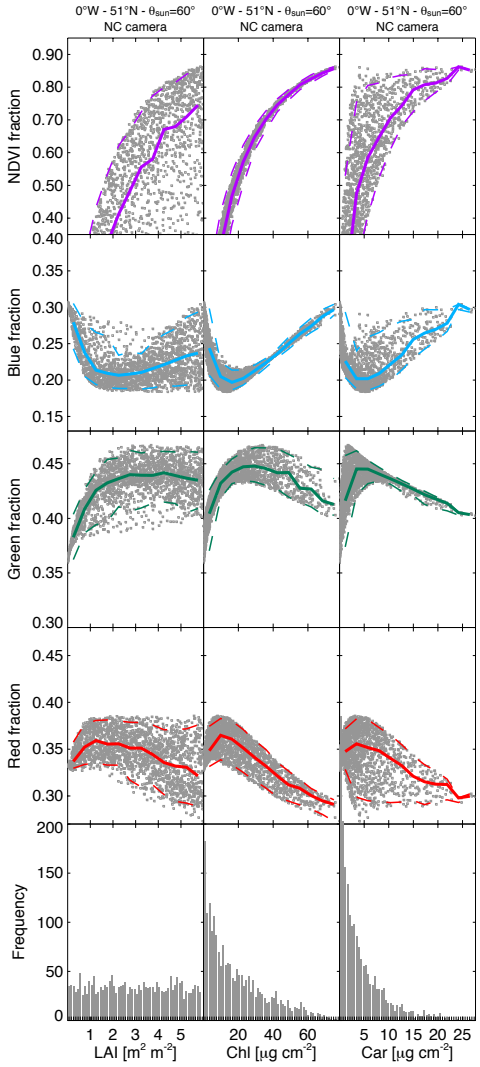

Figure 11. Sensitivity of modelled RGB fractions and NDVI for the NetCam camera at the Alice Holt deciduous broadleaf forest, as predicted by the PROSAIL model and using constrained by Chl:Car and Chl:LAI ratios (see text and compare to those in Fig. S7). All other parameters are set to standard budburst values and the solar elevation is fixed at 60°. The NDVI is computed using the camera view angle and the same wavebands as for MODIS NDVI (545-565 nm for red and 841-871 nm for near infrared). The bottom panel represents the frequency of estimates for a given value of

1 a particular parameter. One can see that compared with Fig. S7 there are more likely
2 to be values skewed to the lower pigment concentrations with our constraints
3 compared with the no constraints analysis of Fig. S7.
4
5

Figure 12

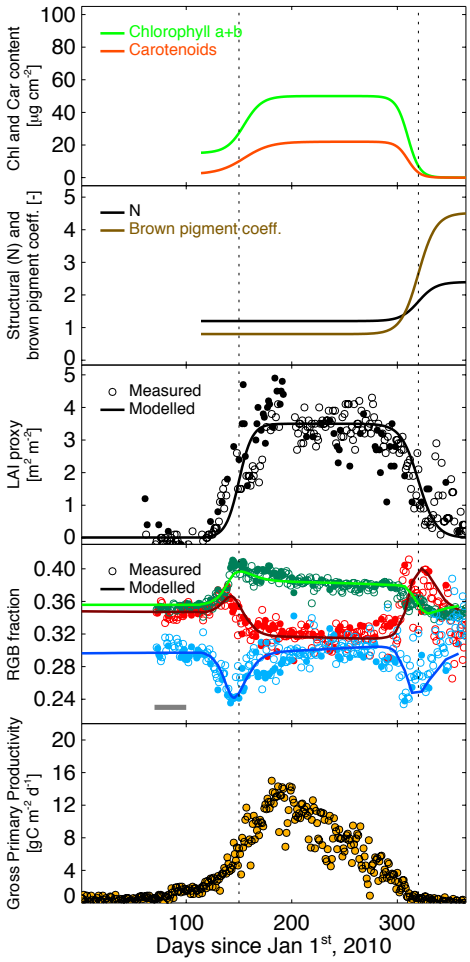

Figure 12. Time-series of modelled leaf chorophyll (Chl), carotenoid (Car) and brown pigment (C_{brown}) contents, leaf structural parameters and modelled LAI used to predict RGB color fractions at the Alice Holt broadleaf deciduous forest for the Netcam camera and the 2010 growing season. Other parameters are as in Table 2. Proxy LAI estimates and measured RGB fractions from camera images are also shown for comparison, as well as measured daily gross primary productivity. Cloud-free conditions (fdiffuse < 0.5) are distinguished from cloudy conditions using closed symbols. The thick grey horizontal bar indicates the period used to adjust B_{RGB} (see

text). The IDL code and data required to generate these figures can be downloaded from the repository (https://bitbucket.org/jerome_ogee/webcam_network_paper).

Figure 13

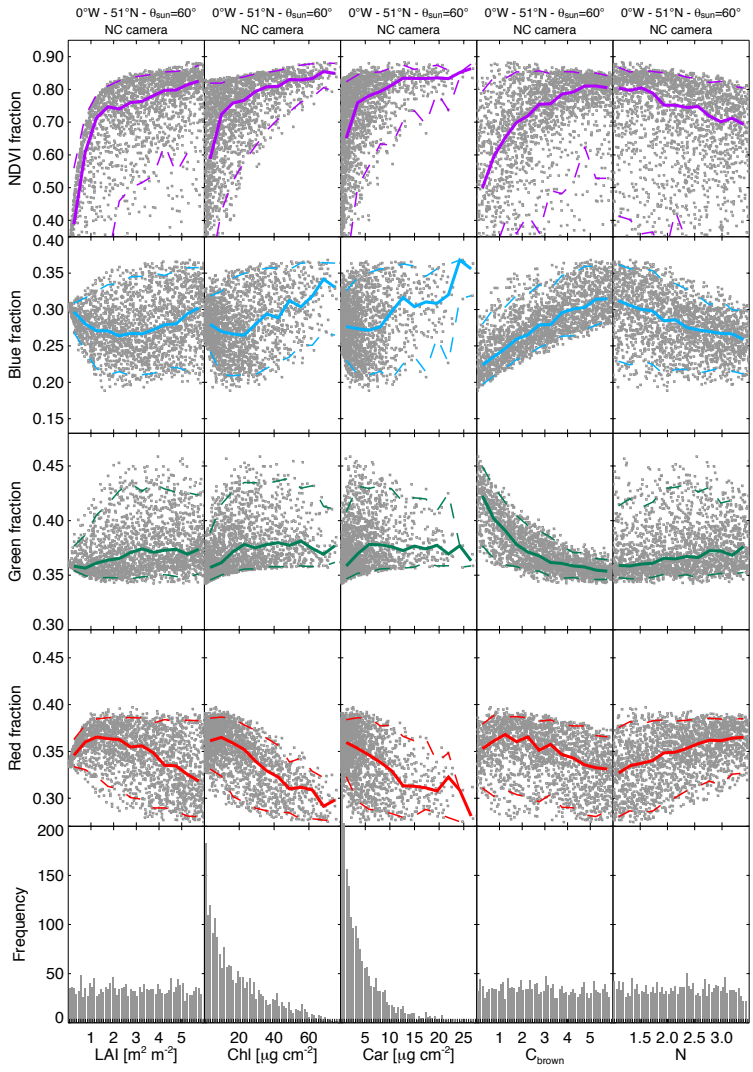

Figure 13. results from the PROSAIL sensitivity analysis as performed in Fig. 12 except that the leaf brown pigment (C_{brown}) and structural paramer (N) are now allowed to vary independantly of the other parameters, as expected during senescence.

Figure 14

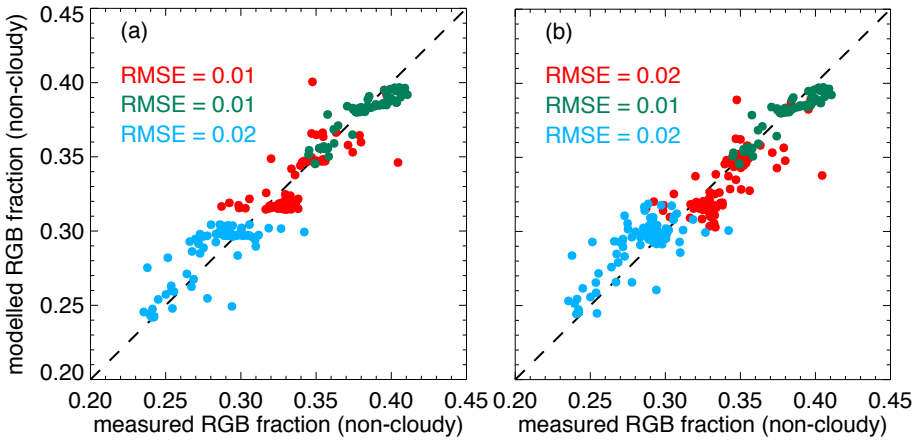

Figure 14. modelled vs. measured RGB fractions for Alice Holt deciduous forest site during cloud-free conditions ($\phi_{diffuse} < 0.5$) assuming (a) constant or (b) variable diffuse light conditions. The modelled values are obtained from the PROSAIL radiative transfer model as described in the text and shown in Fig. 13. The measured RGB fractions are computed from images taken by the Netcam camera system. Similar results were found for the Nikon Coolpix camera.